Available online at www.sciencedirect.com
ScienceDirect
Geochimica et Cosmochimica Acta 70 (2006) 5583–5600
Geochimica
www.elsevier.com/locate/gca

Copper partitioning in a melt–vapor–brine–magnetite–pyrrhotite assemblage

Adam C. Simon [a,*], Thomas Pettke [b], Philip A. Candela [c], Philip M. Piccoli [c], Christoph A. Heinrich [d]

[a] Department of Geoscience, University of Nevada, Las Vegas, NV 89154-4010, USA
[b] Institute of Geological Sciences, University of Bern, Baltzerstrasse 1+3, CH-3012 Bern, Switzerland
[c] Laboratory for Mineral Deposits Research, Department of Geology, University of Maryland, College Park, MD 20742, USA
[d] Isotope Geochemistry and Mineral Resources, Federal Institute of Technology, ETH Zentrum NO, CH-8092 Zurich, Switzerland

Received 7 April 2006; accepted in revised form 18 August 2006

Abstract

The effect of sulfur on the partitioning of Cu in a melt–vapor–brine ± magnetite ± pyrrhotite assemblage has been quantified at 800 °C, 140 MPa, f_{O_2} = nickel–nickel oxide (NNO), $\log f_{S_2} = -3.0$ (i.e., on the magnetite–pyrrhotite curve at NNO), $\log f_{H_2S} = -1.3$ and $\log f_{SO_2} = -1$. All experiments were vapor + brine saturated. Vapor and brine fluid inclusions were trapped in silicate glass and self-healed quartz fractures. Vapor and brine are dominated by NaCl, KCl and HCl in the S-free runs and NaCl, KCl and $FeCl_2$ in S-bearing runs. Pyrrhotite served as the source of sulfur in S-bearing experiments. The composition of fluid inclusions, glass and crystals were quantified by laser-ablation inductively coupled plasma mass spectrometry. Major element, chlorine and sulfur concentrations in glass were quantified by using electron probe microanalysis. Calculated Nernst-type partition coefficients ($\pm 2\sigma$) for Cu between melt–vapor, melt–brine and vapor–brine are $D_{Cu}^{v/m} = 63 \pm 31$, $D_{Cu}^{b/m} = 240 \pm 80$, and $D_{Cu}^{v/b} = 0.27 \pm 0.10$, respectively, in the S-free system. The partition coefficients ($\pm 2\sigma$) for Cu between melt–vapor, melt–brine and vapor–brine are $D_{Cu}^{v/m} = 316 \pm 22$, $D_{Cu}^{b/m} = 443 \pm 68$, and $D_{Cu}^{v/b} = 0.69 \pm 0.16$, respectively, in the S-bearing system. Apparent equilibrium constants ($\pm 1\sigma$) describing Cu and Na exchange between vapor and melt and brine and melt were also calculated. The values of $K_{Cu,Na}^{v/m}$ are 34 ± 21 and 128 ± 29 in the S-free and S-bearing runs, respectively. The values of $K_{Cu,Na}^{b/m}$ are 33 ± 22 and60 ± 5 in the S-free and S-bearing runs, respectively. The data presented here indicate that the presence of sulfur increases the mass transfer of Cu into vapor from silicate melt. Further, the nearly threefold increase in $D_{Cu}^{v/b}$ suggests that Cu may be transported as both a chloride and sulfide complex in magmatic vapor, in agreement with hypotheses based on data from natural systems. Most significantly, the data demonstrate that the presence of sulfur enhances the partitioning of Cu from melt into magmatic volatile phases.

1. Introduction

Copper in porphyry-type ore deposits is generally accepted to have precipitated from magmatic-hydrothermal aqueous fluid(s) evolved from magmatic volatile phases exsolved from magma (Holland, 1972; Whitney, 1975; Burnham, 1979; Candela and Holland, 1984; Dilles, 1987; Hedenquist and Lowenstern, 1994; Candela and Piccoli, 1995; Cline, 1995). This genetic link is based on numerous studies detailing the close association between ore-stage mineralization and aqueous fluid inclusions, interpreted to have been trapped at near magmatic-conditions based on homogenization temperatures up to 700 °C (Roedder, 1972, 1984; Henley and McNabb, 1978; Eastoe, 1982; Hedenquist and Lowenstern, 1994; Candela and Piccoli, 2005). Aqueous fluid inclusion assemblages associated with Cu mineralization are characteristically comprised of both low-salinity aqueous vapor and higher-salinity aqueous brine. Candela and Holland (1984) demonstrated experimentally that Cu partitioning from silicate melt into a magmatic volatile phases is a positive function of the Cl

* Corresponding author.
E-mail address: adam.simon@unlv.edu (A.C. Simon).

0016-7037/$ - see front matter © 2006 Published by Elsevier Inc.
doi:10.1016/j.gca.2006.08.045

concentration of the aqueous phase and, thus, high-salinity brine has been advocated as the dominant Cu-transporting agent in magmatic-hydrothermal systems. However, data from natural fluid inclusions published over the past 15 years have sparked a debate on the relative roles of vapor and brine in scavenging and transporting Cu from silicate melt into the superjacent magmatic environment. The debate centers on the inability to reconcile the partitioning behavior of Cu in many natural boiling assemblages with extant experimental data.

Candela and Holland (1984) studied experimentally the relationship between Cu and Cl in aqueous, supercritical fluids. Their experiments at 750 °C and 140 MPa quantify the partitioning behavior of Cu between silicate melt and saline, aqueous (NaCl–KCl–H_2O), supercritical fluid, exsolved from melt upon crystallization and/or decompression. Candela and Holland (1984) report a linear correlation between the Cu and Cl concentrations of the aqueous fluid over a total chlorinity range from 0 to approximately 5 molal. The linear relationship between Cu and Cl indicates that Cu is most likely transported as the neutral $CuCl^0$ complex in Cl-bearing magmatic-hydrothermal fluids at the pressure-temperature (PT) conditions relevant to the magmatic evolution of porphyry systems. To understand the relative effects of vapor and brine, Williams et al. (1995) equilibrated haplogranite melt with coexisting aqueous, NaCl-, KCl-, HCl-, CuCl- vapor and brine at 800 °C and 100 MPa and 850 °C and 50 MPa. Williams et al. (1995) use apparent exchange equilibria for Cu and Na between the quenched experimental fluid and silicate melt, $D_{Cu,Na}^{aqb/aqv}$, where aqb and aqv are brine and aqueous vapor, respectively, to calculate Nernst-type partition coefficients for Cu between co-existing vapor and brine. They report model brine/vapor partition coefficients for Cu, $D_{Cu}^{b/v}$, of 120 at 100 MPa and 800 °C and 200 at 50 MPa and 850 °C.

Lower temperature studies agree with those performed at magmatic conditions. Pokrovski et al. (2005) investigate metal vapor–liquid partitioning between 350 and 450 °C along the vapor–liquid equilibrium curve in a H_2O–NaCl–KCl–HCl assemblage. The assemblage ranged from pure H_2O to salt saturation with HCl varied from 0 to 0.5 molal. The concentration of Cu in their experiments was found always to be greater in the saline liquid relative to the low-salinity vapor. These experimental data demonstrate that Cu partitions strongly into a high-salinity, Cl-rich brine relative to low-salinity vapor in model NaCl–KCl–HCl–CuCl–H_2O fluid systems. Further, these data provide strong support for the leading role of Cl-bearing aqueous fluids in the evolution of Cu-porphyry deposits. However, extant experimental data do not explain an increasingly ubiquitous characteristic of natural vapor–brine boiling assemblages in porphyry environments: higher Cu concentrations in low-salinity vapor relative to co-existing hypersaline brine.

Recent analyses of individual vapor and brine fluid inclusions from natural boiling assemblages by using micro-analytical techniques suggest that Cu sometimes partitions preferentially into low-salinity vapor relative to co-existing brine. Proton-induced-X-ray-emission (PIXE) and laser-ablation inductively coupled-mass-spectrometry (LA-ICPMS) analyses of co-existing vapor and brine fluid inclusions associated intimately with granite-hosted mineralization in the Yankee Lode deposit (Mole Granite, Australia) indicate that the vapor contains a higher Cu concentration that the brine (Heinrich et al., 1992; Audetat et al., 1998). If the brine was in equilibrium with the vapor at the time of trapping, the data yield a calculated apparent partition coefficient $D_{Cu}^{v/b}$ of 10. Fluid inclusions from the magnetite-rich core to potassic Cu–Au ore at Bajo de la Alumbrera yield a $D_{Cu}^{v/b}$ of approximately 4 (Heinrich et al., 1999; Ulrich et al., 1999). Boiling assemblages in the high-grade Cu–Au zone at Grasberg yield and average $D_{Cu}^{v/b}$ of 4 (Ulrich et al., 1999). Vapor and brine fluid inclusions in the Batu Hijau Cu–Au deposit (Indonesia) contain 2.5 and 0.15 wt% Cu, respectively, yielding a $D_{Cu}^{v/b}$ on the order of seventeen (Ryan et al., 2001). Baker et al. (2004) report Cu concentrations in co-existing vapor and brine from the Bismark deposit (Mexico) that yield a calculated $D_{Cu}^{v/b}$ of approximately 4. Heinrich et al. (1992) use charge balance to demonstrate that the average Cl concentration in vapor fluid inclusions is insufficient to balance the heavy-metal budget of vapor fluid inclusions and they demonstrate that the fractionation of Cu into vapor is not an artifact of the analytical technique. Thus, the strong enrichment of Cu in the vapor phase cannot result solely from volatile $CuCl^0$. Thus, metal complexation must be related to aqueous components other than just Cl. Sulfur is a prime candidate owing to its high concentration in volcanic gases (Hedenquist and Lowenstern, 1994) and strong fractionation into vapor relative to co-existing brine (Drummond and Ohmoto, 1985). Heinrich et al. (1999) cite the presence of up to 1 wt% S in vapor inclusions associated with mineralization in the Yankee Lode as evidence that a S ligand (e.g., H_2S, HS^- or SO_2) may be responsible for the observed fractionation of Cu into the vapor phase.

The data discussed above demonstrate that Cu partitioning in a S-bearing vapor–brine–melt assemblage remains unconstrained. The is driven by the complete lack of experimental data constraining the effect of S on Cu partitioning at magmatic PT-composition (PTX) conditions. Thus, the physico-chemical behavior of Cu during the magmatic stages of porphyry development remains unconstrained. Here we report the first experimental data, to our knowledge, elucidating the effect of S on the partitioning behavior of Cu at the PTX conditions relevant to degassing and concomitant metal transfer from shallow-level felsic melts to exsolved, aqueous vapor and brine. The effect of S is evaluated by assessing the change in the partitioning behavior of Cu with and without the presence of S in a Cl-bearing melt–vapor–brine ± oxide ± sulfide assemblage. Results from experiments at a single set of physico-chemical conditions are presented. These data demonstrate conclusively that S has a pronounced effect

on Cu partitioning behavior. Further experiments are in progress to evaluate the effect of varying oxygen (f_{O_2}) and sulfur (f_{S_2}, f_{H_2S}) fugacities on Cu partitioning. The experimental conditions are similar to those of Candela and Holland (1984) and Williams et al. (1995) and, thus, we include their data for discussion. In this paper we assume the Cu-species in the magmatic volatile phases is dominated by the neutral $CuCl^0$ complex based on experimental studies at similar *PTX* conditions (Candela and Holland, 1984; Williams et al., 1995) and theoretical studies by using HKF equation-of-state calculations for copper(I) chloride species (Liu and McPhail, 2005).

2. Procedures

2.1. Starting materials

A synthetic haplogranite glass with the composition of a 100 MPa haplogranite minimum melt, $Qz_{0.38}Ab_{0.33}Or_{0.29}$ on an anhydrous basis, was used as the starting melt composition. The composition of the glass was determined by XRF and is presented in Table 1. Well-characterized Santa Eulalia pyrrhotite was used as the S source in all S-bearing experiments (Table 2). Starting aqueous solutions were prepared by using doubly deionized and distilled water with reagent grade KCl and NaCl and aqueous HCl to a total salinity of 20 wt% NaCl eq. Cu was added as reagent grade copper(I) chloride (Alfa Aesar, 99.999% metals basis) to the starting solution for runs 7, 8 and 14. There was no Cu added purposely to runs 4, 5 or 6. As discussed below, all run product glasses and fluid inclusions were analyzed by using the same LA-ICPMS element suite and Cu was detected in the fluid inclusions and glasses in run products from experiments 4, 5 and 6. Analyses of lab water used to prepare starting solutions reveal no Cu at detection limits of 0.1 μg/g. Electron microprobe analyses of the capsule material and the starting glass indicate that Cu is present heterogeneously in the capsule material. Thus, trace amounts of Cu heterogeneously distributed in the capsule served as the source of Cu in these runs. Note that the source of Cu is inconsequential to this study. The data for these runs are presented to demonstrate that partition coefficients do not change with significant changes in Cu concentration, spanning two orders of magnitude, of vapor, brine and melt. HCl molarity (11.66 M) was determined by titration. A molar ratio of Na:K:H of unity was used in the starting solutions. The Cu concentration of starting solutions for S-free runs 7, 8 and 14 was approximately 5000 μg/g. No Cu was added to the starting solution in S-bearing runs. Rather, Santa Eulalia pyrrhotite (Hewitt, 1968) obtained from the Smithsonian Institution, Washington, DC, was used as the source of Cu in the S-bearing runs. The starting pyrrhotite contains approximately 2500 μg/g Cu. The starting melt:aqueous fluid mass ratio was added to all capsules at a mass ratio of 1:2.5 in all S-free runs. The starting melt:aqueous fluid:pyrrhotite was added to all capsules at a mass ratio of 1:2.5:0.5 in all S-bearing runs. Prefractured quartz chips were prepared from transparent, inclusion-free quartz from Minas Gerais, Brazil (obtained from the Harvard Mineral Museum). Quartz chips were cut to dimensions of approximately 1.5 cm length by 3 mm width and heated to 350 °C for 30 min and immediately transferred into a room-temperature bath of doubly deionized, distilled water. Immersion in the water bath produces a pervasive fracture network through the chip. The chips were removed from the water bath and dried in a 110 °C oven for 24 h to remove adsorbed water from crack surfaces.

Table 1
Starting composition of synthetic haplogranite

Oxide	wt%
SiO_2	75.18
Al_2O_3	11.09
K_2O	4.43
Na_2O	3.67
CaO	0.17
Fe_2O_3	0.04
MnO	0.01
MgO	0.10
TiO_2	0.03
P_2O_5	0.03
LOI	4.51
Total	99.26

Chemical composition of the starting glass used in all experiments as determined by XRF (Frank, 2001). LOI, loss on ignition. Fe_2O_3 represents total Fe; XRF does not provide information on the Fe^{2+}/Fe^{3+} ratio in the sample.

Table 2
Starting composition of Santa Eulalia pyrrhotite; determined by XRF

Element	Detection limit (μg/g)	Concentration in sample (μg/g)
Ag	0.4	3.9
Al	100	200
Cu	1	2500
Mg	100	700
Mn	1	184
Mo	2	BDL
Ni	1	9
P	NA	20
Pb	4	48
Sr	1	2
V	2	2
Y	2	4
Zn	1	272

NA, not analyzed; BDL, below detection limit.
Data from Stuller (2001).

2.2. Experimental design

An experimental design permitting entrapment of coexisting vapor and brine as fluid inclusions in both pre-fractured quartz chips and in silicate glass at 800 °C and 140 MPa was used. S-free experiments were performed in Pt capsules (4.8 mm ID, 5 mm OD, 30 mm length) loaded with 40 mg synthetic haplogranite glass and 100 μL of

starting aqueous solution. Synthetic, S-free fluid inclusions were trapped in silicate glass as the melt cooled through the glass transition temperature. The method of trapping volatile phases as glass-hosted fluid inclusions was attempted to determine if glass could be used as a suitable container for fluid inclusion LA-ICPMS analyses and also to eliminate any ambiguity with respect to the timing of fluid inclusion formation in pre-fractured quartz (Hanley et al., 2005; Simon et al., 2006). Simon et al. (2006) demonstrate that quartz-hosted fluid inclusions do trap volatile phases which had reached chemical equilibrium with respect to the system. The method of fluid inclusion entrapment (i.e., quartz vs. glass-hosted bubbles) does not affect the experimental results. The S-bearing runs were performed by using Au capsules loaded with 40 mg synthetic haplogranite glass, 20 mg of pyrrhotite, a prefractured quartz chip, and 100 μL of starting aqueous solution. Gold capsules were used for the S-bearing runs to avoid the alloying of S with the noble metal capsule which can mechanically weaken the capsule and potential induce melting of the Au capsule. The choice of capsule material does not affect the experimental results; as discussed below the thickness of the Au capsule is sufficient to allow the achievement of osmotic equilibrium between the capsule contents and the pressure reservoir within 24 h. Fluid inclusions were trapped in self-healing quartz fractures and also in glass. The loaded capsules were placed in dry ice and welded shut. Sealed capsules were weighed, then heated at 110 °C for 4 h and reweighed to verify mechanical integrity via no loss of mass. Single capsules were placed inside René-41 pressure vessels and pressurized with water. The cold-seal vessels were heated inside doubly wound tube furnaces. Charges were first pressurized to 100 MPa, then heated to 800 °C, and then pressurized to the final run pressure. Temperatures were measured with type K (Chromel–Alumel) external thermocouples that were calibrated against internal thermocouples in the presence of the water-pressure medium for each experimental vessel. The furnaces were tilted such that the hot end of the vessel was maintained at a 10° angle from horizontal. This design minimizes the thermal gradient across the charge producing a maximum thermal gradient of ± 5 °C from the hot-spot located at the center of the 3 cm long capsule. Thermal gradients were determined in the presence of the water-pressure medium. The combination of a tilted vessel position and low thermal gradient retards thermal convection in the charge and, thus, inhibits premature healing of cracks in the quartz chips and chemical potential gradients.

An air-driven water-pressure intensifier was used to impose pressure on the charge. Pressure was monitored with Bourdon-tube gauges (±2 MPa) which have been calibrated against factory-calibrated Heise gauges. Experiments were quenched isobarically along a two-stage cooling path involving air-stream cooling from 800 to 200 °C over a period of approximately 2 min followed by immediate immersion in an ambient-temperature water bath. Capsules were removed from the vessels, cleaned, examined microscopically, and weighed to determine if the capsules remained mechanically closed during the experiment. Only capsules that exhibited no mass change greater than 3 mg were processed for analysis.

2.3. Fugacities of H_2, O_2, S_2, SO_2 and H_2S

The values of f_{O_2}, f_{H_2}, f_{S_2}, f_{H_2S} and f_{SO_2} were calculated by using two separate thermodynamic models. The first method uses the equations and methodology of Whitney (1984) and the second follows Clemente et al. (2004, Dr. Bruno Scaillet kindly provided a spreadsheet for this purpose). Thermal dissociation of the water pressure medium yields hydrogen and oxygen via the equilibrium:

$$H_2O = H_2 + 0.5O_2 \quad (1)$$

with the corresponding equilibrium constant:

$$K_w = \frac{f_{H_2} * (f_{O_2})^{0.5}}{f_{H_2O}} \quad (2)$$

The reaction of oxygen with the René-41 vessels, a Ni-based alloy, establishes an intrinsic oxygen fugacity at NNO via the equilibrium:

$$Ni + 0.5O_2 = NiO \quad (3)$$

We have measured the f_{O_2} in René-41 vessels by using the hydrogen sensor technique (Ag–AgCl; H_2O–AgCl) as described by Chou (1987a). The determined value for $\log f_{O_2}$ is -14 ± 1 at 800 °C and 140 MPa. The ensuing establishment within 24 h of osmotic equilibrium between the charge and the pressure buffer imposes a hydrogen fugacity on the charge equal to the NNO oxygen fugacity buffer. The fugacities of oxygen and hydrogen are related through Eqs. (4) and (5). The fugacity of hydrogen, f_{H_2}, was calculated by using the equations of Huebner and Sato (1970) and Belonoshko et al. (1992). The value of $f_{H_2} = 6.2$ at the experimental conditions. The fugacity of water was calculated by using the model of Burnham (1979). The f_{S_2} is constrained to lie along the magnetite–pyrrhotite curve at a fixed f_{O_2}. The fugacity of sulfur, f_{S_2}, calculated according to Whitney (1984) is $\log f_{S_2} = -3.0$. The fugacities of H_2 and S_2 are related directly to the f_{H_2S} via the equilibrium:

$$0.5S_2 + H_2 = H_2S \quad (4)$$

Using the equations in Whitney (1984) yields a value of $\log f_{H_2S} = 1.3$. The fugacities of O_2 and S_2 are related directly to the f_{SO_2} via the equilibrium:

$$0.5S_2 + O_2 = SO_2 \quad (5)$$

Following the equations in Whitney (1984), the value of $\log f_{SO_2} = -1.0$ at run conditions.

The model of Clemente et al. (2004) was also used to calculate values of f_{O_2}, f_{H_2}, f_{S_2}, f_{H_2S} and f_{SO_2}. Interested readers are encouraged to read their paper for specifics of the thermodynamic model. Their model calculates f_{S_2}, f_{H_2S}, f_{SO_2} at fixed P, T, sulfur concentration of the glass, f_{O_2}

and f_{H_2O}. The following values were obtained: $\log f_{O_2} = -14.0$; $f_{H_2} = 6.57$; $\log f_{S_2} = -2.99$; $\log f_{H_2S} = 1.15$ and $\log f_{SO_2} = -1.51$.

2.4. Demonstration of equilibrium

In the present study we use time invariance of the partition coefficients in a closed system to demonstrate equilibrium. The lack of significant change in Cu partitioning behavior with run times varying from 100 to 600 h is interpreted to reflect equilibrium among aqueous fluids, melt and crystals. There was no variation in equilibration time in the runs which contained trace quantities of Cu sourced from the capsule nor the runs to which Cu was added to the starting aqueous solution. Simon et al. (2006) present an comprehensive discussion of the attainment of equilibrium in experiments in which prefractured quartz and rhyolite glass are used to trap aqueous fluids at run PTX conditions and readers are directed to that publication for more details. They conclude that the major and minor-element solute loads both quartz-hosted and glass-hosted fluid inclusions represent equilibrium concentrations trapped at run conditions.

2.5. Run product characterization

The run products from the S-free experiments consisted of a single bead of glass and aqueous vapor. No solid material, other than the glass bead, was recovered from S-free experiments. The S-bearing run products consisted of glass, magnetite, pyrrhotite, aqueous solution and the quartz chip. Magnetite is produced at the experimental PT conditions by the breakdown of pyrrhotite via the reaction:

$$3FeS^{po} + 4H_2O \rightarrow Fe_3O_4^{mt} + 3H_2S + H_2 \quad (6)$$

where po and mt are pyrrhotite and magnetite, respectively. The presence of pyrrhotite in the experimental run-products indicates that pyrrhotite is a stable phase at run conditions, in agreement with previous studies (Lynton et al., 1993; Jugo et al., 1999). Glass recovered from the S-bearing and S-free charges contains both vapor and brine fluid inclusions distributed homogeneously throughout the glass volume (Fig. 1a). The quartz cores recovered from the S-bearing experiments contain both vapor and brine fluid inclusions (Fig. 1b). The presence of vapor fluid inclusions in glass from all run products indicates that vapor was freely distributed throughout the entire capsule at run conditions. The proportion of vapor to brine along the length of the quartz core was not quantified; however, the presence of boiling assemblages was noted along the length of the core and this suggests that vapor was present throughout the capsule. The phase proportions of vapor and brine in both glass and quartz are consistent within individual runs and among all runs. More detailed characterization of quartz-hosted and glass-hosted fluid inclusions will be addressed below.

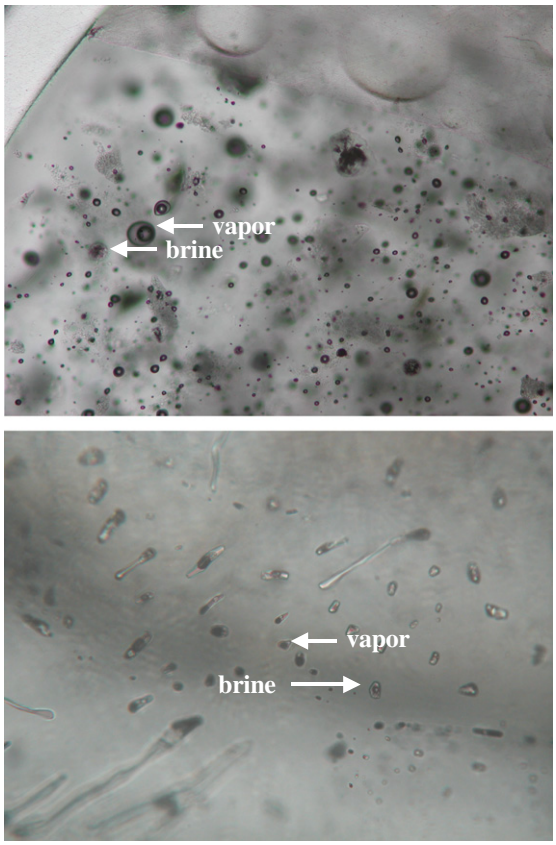

Fig. 1. (a) Photomicrograph of vapor and brine fluid inclusions trapped quenched silicate melt (i.e., glass). in self-healed quartz fractures. (b) Photomicrograph of vapor and brine fluid inclusions trapped in self-healed quartz microfractures. Note the spherical outline of the glass (quenched melt) in the upper left corner of 1a.

2.6. Analytical procedures

2.6.1. Analyses of experimental glasses

A JEOL JXA 8900 electron microprobe equipped with five wavelength dispersive spectrometers (WDS) was used to characterize quantitatively the major element, Cl and S concentrations of run-product silicate glasses. Glass samples were mounted, polished successively to a final diamond grit of 1 μm, and coated with a ~0.03 μm carbon film by using a standard thermal evaporation technique. Operating conditions for glass analyses were 15 keV accelerating potential, 5 nA beam current, and a 15 μm beam size with a minimum counting time of 20 s (sum of peak and background). Multiple line traverses were performed on each glass to evaluate melt homogeneity for both major and minor elements. Individual analyses which yielded anomalously high Cl concentrations were eliminated as these represent the analysis of glass + a vapor fluid inclusion. Analyses were also performed to evaluate the effects of sodium diffusion and silicon and aluminum burn-in (Morgan and London, 1996 and Acosta-Vigil et al., 2003). No systematic migration of sodium was observed in glasses. Standardization for Si, Al, Na and K was performed with a Yellowstone haplogranite (National Museum of Natural History,

NMNH 72854 VG568). Kakanui hornblende was used as the standard for Fe. Scapolite (Meionite, Brazil, USNM R6600-1) was used to standardize Cl and S. Detailed information for standards is located at http://nvl.nist.gov/pub/nistpubs/jres/107/6/j76jar.pdf.

The Cu concentration of silicate glass was quantified by LA-ICPMS. Spots petrographically devoid of fluid inclusions, po and mt crystals were analyzed with a 90 μm spot size. The Cu content of glass volumes directly above and below analyzed fluid inclusions was also quantified. The data suggest that Cu is homogeneously distributed throughout the melt. NBS-610 was used as the reference silicate glass standard and the Si concentrations of glass, determined by EPMA, were used as the internal standard to calculate absolute Cu concentrations. The concentration of major elements in the glass determined both by LA-ICPMS and EPMA overlap at the 2σ uncertainty level.

2.6.2. Fluid inclusion microthermometry

Sulfur-free glass-hosted fluid inclusions in the same glass fragment which we analyzed by EPMA were studied microthermometrically. Following EPMA, the carbon coat was removed by diamond polishing to enhance transparency. Sulfur-bearing vapor and brine trapped in self-healed fractures in the quartz chip were studied microthermometrically. No S-bearing glass inclusions were analyzed microthermometrically. Quartz chips were recovered from experiments and cleaned by agitation in distilled water for 30 min to remove surficial contaminants. Individual chips were set in Crystal Bond and sectioned longitudinally into small discs approximately 500 μm thick. The chips were doubly polished for petrographic examination, microthermometry and LA-ICPMS analysis. Petrographic observation of quartz- and glass-hosted fluid inclusion populations indicates that all runs were vapor and brine saturated with both inclusion types present in each fluid inclusion host. Filling ratios for all fluid inclusions are constant throughout fluid inclusions populations in all runs. Salinities of vapor and brine inclusions were determined by freezing-point depression (i.e., Tm_{ice}) and final dissolution of halite (i.e., Td_{NaCl}), respectively (Bodnar and Vityk, 1994). Measurements were made with a USGS-type gas-flow heating–freezing stage manufactured by Fluid, Inc. The thermocouple was placed directly on top of the sample to prevent sample movement and to minimize the distance between the thermocouple and fluid inclusions. The salinity values reported are the range for all fluid inclusions in each run. There were no systematic differences observed in the microthermometry data of S-free and S-bearing fluid inclusions.

2.6.3. LA-ICPMS analyses of synthetic fluid inclusions

The metal concentrations of individual fluid inclusions were quantified by LA-ICPMS following the methods outlined previously in Günther et al. (1997, 1998), Heinrich et al. (2003), Pettke et al. (2004) and Simon et al. (2004, 2005). Analyses of fluid inclusions in quartz targeted inclusions in multiple healed fractures over the entire length of the quartz chip to evaluate the homogeneity of fluid inclusion solute loads. Similarly, we targeted glass-hosted fluid inclusions throughout the glass volume. A representative LA-ICPMS signal is shown in Fig. 2. This glass-hosted brine inclusion (44 wt% NaCl eq.) measured 15 μm in widest dimension and was ablated from a depth of approximately 25 μm. Transient analytical signals were integrated, and element ratios (e.g., Na:Cu) were quantified by using the NIST silicate glass standard reference material NBS-610. The use of glass standards to quantify the solute load of fluid inclusions has been demonstrated by Günther et al. (1998). Element ratios were transformed into absolute element concentrations by using sodium as the internal standard (Heinrich et al., 2003). The assumption is discussed at length in Heinrich et al. (1992, 2003). Note that element ratios and calculated partition coefficients are independent of this assumption. Therefore, the use of partition coefficients and exchange equilibria to evaluate Cu partitioning behavior is justified. The K concentrations reported for S-free, glass-hosted fluid inclusions display large variation owing to the large mass contribution of K from the glass. This results in a large host correction during signal processing. The quartz-hosted fluid inclusions do not suffer from this problem as the low K concentration in quartz contributes minimally to the fluid inclusion signal interval. Similarly the low Cu concentration in both glass and quartz indicate that the final Cu concentrations are not affected by contributions from the fluid inclusion host.

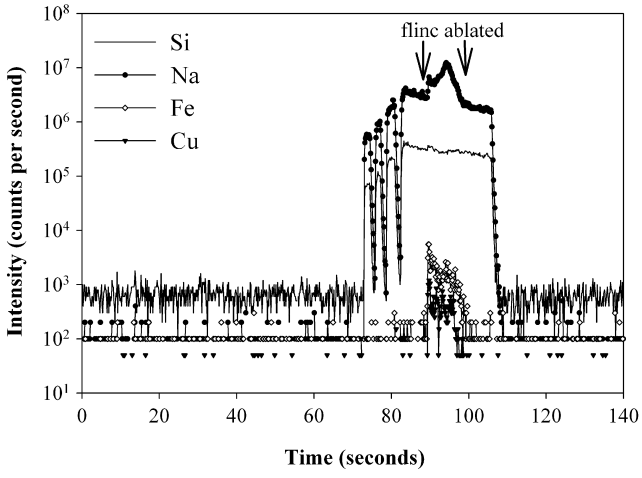

Fig. 2. LA-ICPMS transient signal of a brine fluid inclusion (~35 μm across; 44 wt% NaCl eq.) hosted within glass. A 40 μm beam diameter was used to ablate the entire inclusion. Ablation of glass began at ~73 s and the fluid inclusion was liberated from ~89 to 100 s. Note that the Cu is fully contained inside the fluid inclusion. The two jumps in intensity from 73 to 83 s result from step openings involving a real-time increase in the beam diameter during the analysis.

3. Results

3.1. Metal concentrations in vapor, brine and melt

3.1.1. Fluid inclusions

The metal concentrations, bulk salinities and HCl concentrations of S-free vapor and brine fluid inclusions are presented in Table 3. Metal concentrations and salinities of S-bearing vapor and brine fluid inclusions are presented in Table 4. The reported salinities agree well with predictions based on extant studies (Bodnar et al., 1985; Chou, 1987b; Anderko and Pitzer, 1993). The HCl concentrations of S-free magmatic volatile phases were calculated following Williams et al. (1997) by using their equation:

$$\log\frac{\mathrm{NaCl}^{\mathrm{mvp}}}{\mathrm{HCl}^{\mathrm{mvp}}} = \log\frac{1}{K_{\mathrm{H/Na}}^{\mathrm{mvp/m}}} \times \frac{C_{\mathrm{Na}}^{\mathrm{m}}}{\sum \mathrm{Alkalies}^{\mathrm{melt}}(\mathrm{ASI}-1)} \quad (7)$$

where mvp stands for magmatic volatile phase, ASI is the aluminum saturation index of the melt (i.e., the molar ratio $Al_2O_3/(Na_2O + K_2O)$) and $K_{\mathrm{H/Na}}^{\mathrm{mvp/m}}$ is defined as

$$K_{\mathrm{H/Na}}^{\mathrm{mvp/m}} = \frac{(C_{\mathrm{H}}^{\mathrm{mvp}} \times C_{\mathrm{Na}}^{\mathrm{melt}})}{(C_{\mathrm{H}}^{\mathrm{melt}} \times C_{\mathrm{Na}}^{\mathrm{mvp}})} \quad (8)$$

(Holland, 1972). Model values for $K_{\mathrm{H/Na}}^{\mathrm{mvp/m}}$ were taken from Williams et al. (1997). The equations above are valid strictly for glasses with ASI > 1 and, thus, only the HCl concentrations of vapor and brine in one S-bearing run (i.e., Po-15) were calculated owing to the slightly peralkaline nature of the two remaining runs. However, based on the initial aqueous solution chemistry, the HCl of these S-bearing volatile phases should be comparable in all S-bearing runs. The HCl concentrations reported here agree with the thermodynamic model of Williams et al. (1997) which shows that an increase in the ASI of the melt, in equilibrium with aqueous vapor and/or brine, should yield a increase in the HCl/NaCl ratio of the volatile phase and that the ratio of HCl/NaCl of the vapor should exceed that of the brine. The data from the current study indicate that the HCl/NaCl molal ratio increases from 0.34 to 9 as the ASI increases from 1.00 (run Po-15) to 1.15 (run 4). Further, the molal ratio of NaCl/HCl in vapor always exceeds that of brine. The change in Cu content from runs 4, 5 and 6 to 7, 8, and 14 reflects the greater mass quantity of Cu present in the starting material of the latter three runs as discussed in Section 2.1. above.

3.1.2. Haplogranite melt

Major element, chlorine and sulfur concentrations are presented in Table 5 and Cu concentrations in Tables 3 (S-free runs) and 4 (S-bearing runs). Silicate glasses recovered from the S-free experiments are peraluminous rhyolites. The increase in ASI from the starting melt composition of 1.01 indicates that the melts lose Na and K to the aqueous fluids at run conditions. The mass transfer of Na and K to the vapor is balanced by the transfer of H from the vapor into the melt. This exchange of Na + K for H does not cause any change in the salinity of the volatile phases. The sulfur-bearing glasses are slightly peralkaline to metaluminous rhyolites indicating minimal exchange of Na and K between the melt and volatile phases.

The average Cu concentration in the S-bearing glasses reported here, $C_{\mathrm{Cu}}^{\mathrm{m}} = 1 \pm 0.1(\pm 2\sigma)$, is an order of magnitude lower than that reported in previous studies involving S-bearing rhyolite melt and pyrrhotite. Lynton et al. (1993) report an average Cu concentration ($\pm 1\sigma$) in rhyolite glass of 43 ± 14 at 800 °C, 100 MPa, $f_{O_2} = \mathrm{NNO} + 0.5$ and $\log f_{S_2}$ values ranging from −1 to −2. Jugo et al. (1999) report an average Cu concentration ($\pm 1\sigma$) in rhyolite glass of 26 ± 3 at 850 °C, 100 MPa, $f_{O_2} = \mathrm{NNO} - 0.25$ and $\log f_{S_2} = -1$. The mass transfer of Cu between melt and pyrrhotite may be represented by one possible equilibrium such as:

$$\mathrm{CuO}_{0.5}^{\mathrm{m}} + \mathrm{FeS}^{\mathrm{po}} + 0.5\mathrm{S}_2 = \mathrm{CuFeS}_2^{\mathrm{po}} + 0.25\mathrm{O}_2 \quad (9)$$

Table 3
LA-ICPMS data for S-free fluid inclusions and melt

Run no.	Run time (h)	Type of inclusions analyzed	Number of inclusions analyzed	Final wt% NaCl eq.	Molality of HCl in volatile phase	Cu in fluid inclusions μg/g ($\pm 2\sigma$)	Na in fluid inclusions μg/g ($\pm 2\sigma$)	K in fluid inclusions μg/g ($\pm 2\sigma$)	Cu in glass μg/g ($\pm 2\sigma$)
4	205.5	Vapor	10	8.3–8.9	0.33	14 (6)	25,000 (4600)	17,000 (5300)	0.48 (0.32)
4		Brine	5	41–44	0.38	52 (24)	79,500 (30,200)	66,000 (30,000)	0.48 (0.32)
5	110	Vapor	9	8.5–9.7	0.32	18 (10)	25,000 (6400)	13,000 (5100)	0.34 (0.18)
5		Brine	7	42–46	0.36	73 (30)	77,000 (12,000)	55,000 (20,000)	0.34 (0.18)
6	377	Vapor	8	9.1–9.4	0.31	22 (12)	22,000 (4800)	12,500 (9000)	0.21 (0.12)
6		Brine	7	42–44	0.20	42 (16)	84,000 (27,000)	47,000 (38,000)	0.21 (0.12)
7	205	Vapor	7	8.7–9.3	0.36	860 (410)	24,000 (3500)	14,000 (4000)	32 (23)
7		Brine	4	42–44	0.40	6900 (600)	90,500 (5600)	114,000 (31,000)	32 (23)
8	110.25	Vapor	8	8.1–9.3	0.29	2100 (800)	21,000 (7700)	38,000 (9500)	26 (15)
8		Brine	5	42–45	0.30	7600 (2600)	86,000 (13,400)	76,000 (26,000)	26 (15)
14	159.5	Vapor	8	8.5–9.3	0.30	900 (450)	24,500 (4400)	23,000 (5500)	10 (6)
14		Brine	8	41–43	0.35	5300 (1050)	87,500 (960)	98,000 (25,000)	10 (6)

HCl concentrations were calculated following Williams et al. (1997) and represent the molarity of HCl in the volatile phase. Runs 7, 8 and 14 contained a high concentration of Cu in the starting aqueous solution, whereas the starting aqueous solution for runs 4, 5 and 6 contained no Cu; Cu in these latter runs was sourced from the capsule material.

Table 4
LA-ICPMS data for S-bearing fluid inclusions

Run no.	Run time (h)	P (MPa)	Type of inclusions analyzed	Number of inclusions analyzed	Final wt% NaCl eq.	Molarity of HCl in the volatile phase	Cu in fluid inclusions μg/g (±2σ)	Na in fluid inclusions μg/g (±2σ)	K in fluid inclusions μg/g (±2σ)	Fe in fluid inclusions μg/g (±2σ)	Cu in glass μg/g (±2σ)
Po-11	236	140	Vapor	5	8.6–9.5	NC[1]	315 (76)	20,200 (2800)	30,000 (6000)	21,000 (7900)	1.0 (0.2)
Po-11		140	Brine	7	41–44	NC[1]	475 (41)	105,000 (4500)	114,000 (9200)	29,000 (7500)	
Po-14	185	140	Vapor	5	8.5–9.4	NC[1]	293 (69)	20,900 (3200)	25,000 (11,000)	21,000 (2300)	1.0 (0.3)
Po-14		140	Brine	8	41–45	NC[1]	467 (52)	106,000 (8900)	110,000 (9000)	35,000 (7900)	
Po-15	359	140	Vapor	5	8.9– 9.8	0.1	371 (98)	20,600 (2700)	33,000 (7200)	19,000 (5600)	0.9 (0.3)
Po-15		140	Brine	5	42-46	0.01	475 (62)	106,000 (7500)	115,000 (9000)	31,000 (6400)	

HCl concentrations were calculated following Williams et al. (1997) and represent the molarity of HCl in the volatile phase. NC, not calculated using the equations from Williams et al. (1997) because the ASI of the glass is less than one rendering the equations unusable.

where Cu is assumed to be present as a Cu-oxide component in the melt. If Cu is present in the melt as a Cu-sulfide component, a similar equilibrium can be written as:

$$CuS^{m}_{0.5} + FeS^{po} + 0.25S_2 = CuFeS^{po}_2 \quad (10)$$

These equilibria show that the partitioning of Cu between melt and pyrrhotite depends on f_{O_2} and f_{S_2} of the environment. The Cu concentrations in pyrrhotite among the different studies vary by a factor of nearly 3; 6900 ± 300 μg/ (Jugo et al., 1999), 2170 ± 520 μg/ (Jugo et al., 1999) and 174 ± 103 μg/g (this study). Thus, the calculated pyrrhotite/melt partition coefficients (±1σ) for Cu, $D^{po/m}_{Cu}$, vary significantly; 550 ± 220 in Lynton et al. (1993), 2600 ± 300 in Jugo et al. (1999) and 174 ± 53. Jugo et al. (1999) related the change in $D^{po/m}_{Cu}$ to changes in f_{O_2} and f_{S_2}. The $\log f_{O_2}$ of −14 in the present study is one-half an order of magnitude lower than that reported by Lynton et al. (1993) and one-quarter of an order of magnitude higher than that reported by Jugo et al. (1999). As discussed in Jugo et al. (1999), the effect of varying f_{O_2} and f_{S_2} on the partitioning of Cu between hydrous rhyolite and pyrrhotite Cu can be expressed by the equation:

$$\log D^{po/m}_{Cu} = \log K + 0.5 \log f_{S_2} + \log a^{po}_{FeS} - 0.25 \times \log f_{O_2} \quad (11)$$

where

$$\log K = \frac{a^{po}_{CuFeS_2} \times (f_{O_2})^{0.25}}{(f_{S_2})^{0.5} \times a^{m}_{CuO_{0.5}} a^{po}_{FeS}} \quad (12)$$

This equation predicts that the value of $D^{po/m}_{Cu}$ should be 2 at a $\log f_{S_2} = -3$ and $\log f_{O_2} = -14$. The new data presented here yield a calculated value of $D^{po/m}_{Cu} = 2.2$ in agreement with the thermodynamic model presented in Jugo et al. (1999). Thus, the lower Cu concentrations in rhyolite glass and pyrrhotite reported here are interpreted to represent equilibrium values at the reported PTX, f_{O_2} and f_{S_2} conditions. The magnetite and pyrrhotite data determined in the present study will be presented, discussed and modeled in a separate publication.

3.1.3. Pyrrhotite and magnetite crystals in S-bearing runs

The concentration of Cu in magnetite and pyrrhotite are presented in Table 6. Magnetite crystals hosted in silicate glass from runs 6, 8 and 14 and pyrrhotite crystals hosted in silicate glass from runs 8 and 14 were analyzed by LA-ICPMS and the transient signals were processed by removing the host contribution to the signal and assuming end-member compositions for each mineral phase; a valid assumption considering the absence of Ti and other solid-solution components. Analyses of magnetite and pyrrhotite in glass were not the primary focus and, thus, only those crystals which were close tot he glass surface were analyzed by LA-ICPMS. While the number of analyses is limited, the data are robust and allow us to place constraints on the partitioning of Cu between magnetite and melt and pyrrhotite and melt at the experimental PTX conditions. A

Table 5
EPMA analyses of major elements, chlorine and sulfur in the run product glasses

P (MPa)	SiO_2 wt% ($\pm2\sigma$)	K_2O wt% ($\pm2\sigma$)	Na_2O wt% ($\pm2\sigma$)	FeO wt% ($\pm2\sigma$)	Al_2O_3 wt% ($\pm2\sigma$)	Cl wt% ($\pm2\sigma$)	SO_3 wt% ($\pm2\sigma$)	Total	ASI
Glass from S-free experiments									
4	76.10 (3.71)	3.93 (0.82)	2.80 (0.53)	0.05 (0.19)	11.57 (1.83)	0.16 (0.03)	NA	94.57	1.31
5	76.45 (2.17)	3.77 (0.37)	2.73 (0.28)	0.03 (0.12)	11.14 (1.00)	0.14 (0.03)	NA	94.23	1.30
6	75.87 (2.26)	3.88 (0.21)	3.05 (0.44)	0.04 (0.14)	11.90 (1.50)	0.11 (0.02)	NA	94.82	1.29
7	76.35 (1.20)	4.98 (0.38)	2.24 (0.41)	0.05 (0.11)	11.43 (0.57)	0.14 (0.02)	NA	95.17	1.26
8	75.76 (2.12)	4.60 (0.51)	2.60 (0.04)	0.05 (0.10)	11.44 (1.01)	0.15 (0.04)	NA	94.91	1.23
14	75.69 (1.53)	4.85 (0.56)	2.39 (0.57)	0.04 (0.19)	11.23 (1.41)	0.16 (0.02)	NA	94.33	1.22
Glass from S-bearing experiments									
Po-11	76.14 (0.90)	5.05 (0.21)	2.16 (0.17)	1.46 (0.61)	8.81 (1.18)	0.20 (0.05)	0.03 (0.06)	93.81	0.97
Po-14	74.08 (1.14)	5.26 (0.59)	2.34 (0.30)	3.26 (1.25)	8.30 (1.53)	0.31 (0.06)	0.01 (0.03)	93.48	0.87
Po-15	75.03 (1.25)	5.25 (0.49)	2.26 (0.33)	1.35 (0.39)	9.42 (1.16)	0.19 (0.03)	0.04 (0.04)	93.49	1.01

Each datum represents the average of a minimum of 10 spot analyses in different areas of a given experimental glass. ASI was calculated as the molar ratio $[Al_2O_3/(Na_2O + K_2O)]$ The calculated values of ASI indicate that all experimental melts were peraluminous to slightly peralkaline. Uncertainties are presented as twice the standard deviation from the mean ($\pm2\sigma$) for the replicate measurements of each glass. NA, not applicable.

Table 6
Cu concentrations (μg/g) in pyrrhotite and magnetite

Run no.	Magnetite ($\pm2\sigma$)	Pyrrhotite ($\pm2\sigma$)
6	BDL; 24.6	NA
6	BDL; 14.4	NA
8	NA	293
8	NA	112
8	4.1 (1.6)	117
8	BDL; 2.1	NA
8	BDL; 2.1	NA
8	BDL; 10.3	NA
14	NA	NA
14	BDL; 14.4	NA
14	4.6 (1.8)	NA
14	BDL; 5.6	NA

NI, not analyzed in the glass run product during LA-ICPMS analysis. BDL, below detection limit and indicates that the Cu concentration in the mineral phase is less than the 3σ limit of detection calculated as described in Longerich et al. (1996); the calculated 3σ LOD is provided for each analysis.

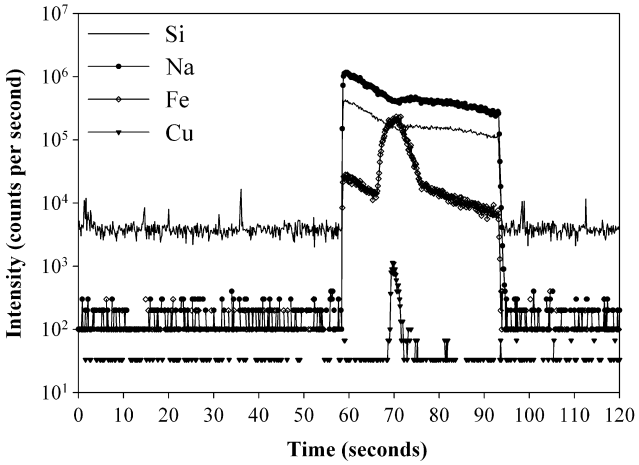

Fig. 3. LA-ICPMS transient signal of a pyrrhotite crystal ablated from silicate glass (i.e., quenched melt). Po is ablated from ~66 to 76 s and Cu is clearly contained within the po crystal.

more extensive discussion of the melt/crystal partitioning data from the current study which constrain the effect of pyrrhotite and magnetite crystallization on the Cu budget of an evolving magmatic system are being published separately. The raw signals for Cu in both magnetite and pyrrhotite indicate that Cu is contained within the analyzed crystal and not present as a surface particle (Fig. 3). The signals were processed with a 3σ limit of detection (LOD) filter (Longerich et al., 1996). This results in relatively high LODs for most magnetite analyses. Processing the signals with a 2σ LOD does not improve the results for magnetite. The large uncertainty for some analyses results from a low mass factor which necessitates large extrapolation from the mixed signal to obtain the absolute Cu concentration in the pure mineral phase (Halter et al., 2002; Simon et al., 2003). Magnetite crystals display a cubic morphology with maximum diameters on the order of 10 μm. The data for magnetite suggest that the concentration of Cu is on the order of a few μg/g. Based on the data presented in Table 6, we suggest that the a reasonable estimate for the Cu concentration in magnetite is 2 μg/g. The Cu concentration in magnetite could be lower as reflected in the 3σ LODs on the order 2 μg/g for two analyses; however, the value of 2 μg/g agrees well with data from natural magnetite–rhyolite assemblages (Ewart and Griffin, 1994). Pyrrhotite crystals display a hexagonal morphology with maximum diameters on the order of 12 μm. The best estimate for the Cu concentration of pyrrhotite is 174 ± 103 μg/g based on analyses of pyrrhotite hosted in glass from run Po-11.

The Cu concentrations in pyrrhotite reported here are considerably lower than those reported in previous experimental studies at similar PT conditions. Lynton et al. (1993) report a mean Cu concentration of 2.17 ± 0.52 wt% in an aqueous-fluid-saturated pyrrhotite–rhyolite assemblage at 800 °C, 100 MPa, $f_{O_2} = NNO + 0.5$ and $\log f_{S_2} = -2$. Jugo et al. (1999) report a mean Cu concentration of 6.9 ± 0.3 wt% in a aqueous-fluid-saturated pyrrhotite-intermediate solid solution-rhyolite assemblage at 850 °C, 100 MPa, $f_{O_2} = NNO - 0.25$ and $\log f_{S_2} = -1$. The presence of intermediate-solid-solution saturates the

Cu concentration of pyrrhotite to the high value reported in Jugo et al. (1999). Stimac and Hickmott (1994) report Cu concentrations of 3014 ± 88 μg/g and 2757 ± 97 μg/g in pyrrhotite microphenocrysts from rhyolite lava samples collected at Clear Lake, CA (USA). They report log f_{S_2} values of −1.25 and −1.97 for the two samples, respectively, determined following Toulmin and Barton (1964). These data from natural pyrrhotite agree well with extant experimental data. There is no reason to suspect the Cu content in starting pyrrhotite is highly heterogeneous and, thus, the lower final pyrrhotite Cu concentrations in this study indicate that pyrrhotite has undergone diffusional re-equilibration at run P and T to cause the Cu concentrations to drop from its initial value of 2583 μg/g to the final value of 174 ± 103 μg/g.

3.2. Cu partitioning between melt, vapor and brine

3.2.1. S-free aqueous fluids and melt

Apparent Nernst-type partition coefficients ($\pm 2\sigma$) describing Cu exchange between vapor and melt, $D_{Cu}^{v/m}$, and brine and melt, $D_{Cu}^{b/m}$, are presented in Table 7. Calculated partition coefficients ($\pm 2\sigma$) for Cu between vapor and melt and brine and melt range from 27 ± 23 to 102 ± 80 and 109 ± 87 to 519 ± 317, respectively (Table 7). The calculated partition coefficients indicate that Cu is partitioned strongly into NaCl–KCl–HCl–H_2O ± $FeCl_2$ fluids at the PTX conditions of the current study. However, the reported partition coefficients are valid strictly for the PTX conditions reported here. Changes in pressure, temperature, gas fugacities, bulk composition, etc. will cause the partition coefficients to change. Thus, in order to compare the new data with those from other studies at different PTX conditions, we calculated apparent equilibrium constants based on the exchange of Cu and Na between the volatile phase and melt. Copper and Na exchange between the melt and vapor and melt and brine can be described by the equilibria:

$$CuO_{0.5}^{m} + NaCl^{v} = CuCl^{v} + NaO_{0.5}^{m} \quad (13)$$

$$CuO_{0.5}^{m} + NaCl^{b} = CuCl^{b} + NaO_{0.5}^{m} \quad (14)$$

Table 7
Partition coefficients ($\pm 2\sigma$) for Cu between coexisting vapor, brine and melt at 800 °C and 140 MPa

Run no.	$D_{Cu}^{v/m}(\pm 2\sigma)$	$D_{Cu}^{b/m}(\pm 2\sigma)$	$D_{Cu}^{v/b}(\pm 2\sigma)$
S-free runs			
4	30 (21)	109 (87)	0.28 (0.14)
5	52 (3)	215 (143)	0.24 (0.12)
6	102 (80)	198 (116)	0.52 (0.30)
7	27 (23)	217 (156)	0.13 (0.06)
8	79 (55)	294 (196)	0.27 (0.14)
14	86 (65)	519 (317)	0.17 (0.09)
S-bearing runs			
Po-11	320 (93)	482 (89)	0.66 (0.17)
Po-14	304 (119)	433 (68)	0.63 (0.16)
Po-15	325 (157)	416 (176)	0.78 (0.32)

Table 8
Calculated values for the exchange of Cu and Na between melt and aqueous volatile phase, either vapor or brine ($\pm 1\sigma$)

Run no.	$K_{Cu,Na}^{v/melt}(\pm 1\sigma)$	$K_{Cu,Na}^{b/melt}(\pm 1\sigma)$
S-free runs		
4	15 (5)	18 (6)
5	27 (6)	36 (9)
6	67 (18)	34 (14)
7	12 (10)	25 (9)
8	42 (39)	8 (11)
14	41 (46)	68 (48)
S-bearing runs		
Po-11	107 (48)	56 (20)
Po-14	115 (51)	60 (34)
Po-15	161 (129)	66 (51)

The calculated values $K_{Cu,Na}^{v/m}(\pm 1\sigma)$ and $K_{Cu,Na}^{b/m}$, are presented in Table 8.

3.2.2. S-free vapor and brine

Calculated partition coefficients ($\pm 2\sigma$) for Cu between vapor and brine range from 0.13 ± 0.06 to 0.52 ± 0.30 with a mean value of 0.27 ± 0.10 (Table 7). These data indicate that Cu partitions preferentially into brine relative to low-salinity aqueous vapor at the experimental conditions reported here. The values of $D_{Cu}^{v/b}$ calculated from the new data are three orders of magnitude higher than those in Williams et al. (1995). They report that $D_{Cu}^{v/b} = 8 \times 10^{-3}$ at 100 MPa and 800 °C. Williams et al. (1995) demonstrate that the value of $D_{Cu}^{v/b}$ increases with decreasing pressure owing to the strong enrichment of total chloride, $\sum_{Cl}$, and HCl in the brine phase and corresponding depletion of $\sum_{Cl}$ and HCl in the vapor. The value of $D_{Cu}^{v/b}$ is constrained to equal unity at the critical pressure (~160 MPa in the NaCl–KCl–HCl–H_2O system) as the concentration of Cu in vapor and brine must approach a common value as the critical pressure is approached along the 800 °C solvus. Thus, the new results at 140 MPa agree with the predication that $D_{Cu}^{v/b}$ will decrease significantly at lower pressure.

3.2.3. S-bearing aqueous fluids and melt

Calculated partition coefficients ($\pm 2\sigma$) for Cu between vapor and melt and brine and melt range from 304 ± 119 to 325 ± 157 and 416 ± 176 to 482 ± 89, respectively (Table 7). The mean value for $D_{Cu}^{v/m}$, 316 ± 11, is at least a fivefold increase from that in the S-free system, $D_{Cu}^{v/m} = 63 \pm 31$, reported here. The Nernst-type Ds provide a simple empirical measure of the distribution of Cu between melt and vapor and melt and brine at the specific set of experimental conditions detailed in the current paper. In order to evaluate the equilibria which control the exchange of Cu between the melt and vapor and melt and brine, apparent exchange constants ($\pm 1\sigma$) for Cu and Na are presented in Table 8. The data indicate that the Na concentrations in S-free and S-bearing glass are consistent at the 2σ uncertainty level and, thus, the variations in Na

do not affect the calculated equilibrium constant values. The use of Eqs. (13) and (14) to describe Cu exchange in the S-bearing system ignores strictly the effect of S on the activities of NaCl and HCl in the vapor and brine and also Cu speciation in the melt. However, considering that the Na and HCl concentrations of the vapor and brine are consistent among the S-free and S-bearing runs, the values calculated using Eqs. (13) and (14) for the S-bearing system provide data with which to evaluate the effect of S on metal exchange. The mean value of the apparent exchange constant in the S-bearing system, $K^{v/m}_{Cu,Na} = 128 \pm 29$, is notably higher than that calculated for the S-free vapor–melt system, $K^{v/m}_{Cu,Na} = 34 \pm 21$. This increase is interpreted to reflect enhanced partitioning of Cu from the melt into aqueous vapor owing to the presence of available sulfur ligands in the latter. The average $D^{b/m}_{Cu}$ is similar, albeit higher, than the value calculated from data in the sulfur free system, $D^{b/m}_{Cu} = 250$. The mean value of the apparent exchange constant ($\pm 1\sigma$) for Cu and Na between brine and melt is $K^{b/m}_{Cu,Na} = 60 \pm 5$. This value is almost twice as high as $K^{b/m}_{Cu,Na}$ calculated from the S-free data set. We infer this increase in the exchange constant to reflect the enhanced partitioning of Cu into S-bearing brine relative to the S-free system.

3.2.4. S-bearing vapor and brine

Calculated partition coefficients ($\pm 2\sigma$) for Cu between vapor and brine range from 0.63 ± 0.16 to 0.78 ± 0.32 with a mean value of 0.69 ± 0.12 (Table 7). The average value for $D^{v/b}_{Cu}$ in the S-bearing system is two and one half times the value determined in the S-free system. There were no additional system components added to the S-bearing runs apart from Cu-bearing pyrrhotite. Sulfur partitions strongly into aqueous vapor relative to brine (Drummond and Ohmoto, 1985) and, thus, we suggest that the increase in $D^{v/b}_{Cu}$ reflects the existence of a Cu–S species in the vapor phase as discussed below.

4. Discussion

4.1. Melt–vapor–brine partitioning

4.1.1. Vapor–brine partition coefficients

Phase relations in the NaCl–KCl–H_2O system, a proxy for more complex magmatically generated aqueous fluids, indicate that at all pressures below approximately 160 MPa, at 800 °C, a vesiculating melt with an initial Cl:H_2O mass ratio on the order of 0.05 will exsolve coexisting vapor and brine (Bodnar et al., 1985; Anderko and Pitzer, 1993; Candela and Piccoli, 1995). The melt will exsolve only low-salinity vapor at lower Cl:H_2O mass ratios, and the Cl concentration of the melt will increase until the melt reaches brine saturation. Average Cl concentrations of melt inclusions in andesite to rhyolitic magmatic systems indicate that most melts undergoing crystallization-induced degassing exsolve aqueous vapor first followed later by brine. The composition of the volatile phases is dominated by NaCl, KCl, and HCl and, thus, previous experimental studies on Cu partitioning from melt into the volatile phase have been performed in systems with these salts (Candela and Holland, 1984; Williams et al., 1995). These studies demonstrate that Cu is strongly coupled to Cl with the concentration of Cu in the aqueous phase(s) increasing linearly with Cl. However, as discussed in the introduction, recent published data from natural fluid inclusion boiling assemblages suggest that Cu may not be transported solely as a chloride complex in magmatic-hydrothermal fluids (Heinrich et al., 1999).

The ability of magmatic volatile phases to carry significant S has been demonstrated by the quantitative study of melt inclusions. Westrich et al. (1991) quantified the S concentration in melt inclusions and matrix glass of an andesite magma and determined that the magma lost considerable S during eruptive degassing. Lowenstern (1993) concludes that the fractionation of sulfides from the andesite could not have produced the significant depletion of S in the andesite. Rather, loss of S to a volatile phase is invoked to explain the order of magnitude difference in the S content of melt inclusions and matrix glass. Values for vapor/brine partition coefficients for Cu, determined from natural fluid inclusion assemblages, range from ~0.5 (Harris et al., 2003) to approximately 100 (Heinrich et al., 1999). Experimental data (Candela and Holland, 1984; Williams et al., 1995) which indicate strong coupling of Cu and Cl suggest that if chloride is the only available Cu-complexing ligand the concentration of Cu should be highest in brine relative to co-existing lower-salinity vapor. That the opposite is found in some natural boiling assemblages indicates the potential presence of a second Cu-complexing ligand which preferentially partitions into the vapor. The element S has been demonstrated to fractionate into the vapor phase during boiling (Drummond and Ohmoto, 1985) and Heinrich et al. (1999) suggest that HS^- complexation may be responsible for the enhanced Cu partitioning into vapor, consistent with predictions based on lower temperature studies of Cu–S complexing (Mountain and Seward, 1999). The new data reported here at magmatic PTX conditions indicate that volatile S does have a pronounced effect on the mass transfer of Cu into low-salinity vapor. The calculated vapor/brine Nernst-type partition coefficient increases from $D^{v/b}_{Cu} = 0.27 \pm 0.14$ in the S-free system to $D^{v/b}_{Cu} = 0.69 \pm 0.16$ in the S-bearing system. However, while these data demonstrate a nearly threefold increase in Cu partitioning into vapor, the Cu concentration of brine remains higher at the PTX conditions of the current study. Thus, the conditions (P, T, f_{S_2}, f_{O_2}, etc.) which yield a $D^{v/b}_{Cu} > 1$ in some natural vapor–brine boiling assemblages (Heinrich et al., 1999) remain unconstrained; additional experiments are planned at different PTX conditions in an attempt to quantify the preferential partitioning into vapor in some natural systems.

The vapor-melt and brine-melt partition coefficients reported here overlap with data reported by Harris et al. (2003) for a natural, hence S-bearing, vapor–brine–melt

assemblage trapped at magmatic conditions in the porphyry-Cu deposit at Bajo de la Alumbrera, Argentina. The assemblage was found in a Cu-Fe sulfide-bearing quartz vein and, thus, the volatile phases should contain S, although S was not part of the PIXE analysis package (Dr. Anthony Harris, personal communication). Partition coefficients were calculated assuming a range of initial Cu concentrations in melt of 50 to 200 μg/g. The values of $D_{Cu}^{v/m}$ reported by Harris et al. (2003) range from 200 to 800 encompasses the mean value, $D_{Cu}^{v/m} = 315 \pm 22$, determined from data in the new study. The value of $D_{Cu}^{b/m}$ ranges from 500 to 2000 and agrees broadly with the value of 443 ± 68 reported here. The strong agreement between the new data reported here and a natural vapor–brine–melt assemblage from a world-class Cu-porphyry deposit suggests that our partitioning data provide the best current estimate for the behavior of Cu at magmatic PTX conditions.

4.1.2. Thermodynamic exchange constants

Here we discuss the apparent exchange constants for Cu and Na between vapor and melt ($K_{Cu,Na}^{v/m}$) and brine and melt ($K_{Cu,Na}^{b/m}$). These data are presented in Table 8. The value of $K_{Cu,Na}^{v/m} = 34 \pm 21(1\sigma)$ in the S-free vapor–melt system compared with $K_{Cu,Na}^{v/m} = 128 \pm 29(1\sigma)$ in the S-bearing vapor–melt system. The nearly fourfold increase in the value of $K_{Cu,Na}^{v/m}$ occurs in the absence of significant changes in the sodium concentrations of vapor or melt. Thus, the increase in $K_{Cu,Na}^{v/m}$ is interpreted to reflect the presence of sulfur in the vapor phase. These data suggest that the presence of S affects the mass transfer of Cu from the melt into the vapor. Likewise, the nearly twofold increase in $K_{Cu,Na}^{v/m}$ also suggests the presence of a Cu–S complex in the brine. In combination with the simple Nernst-type partition coefficients presented and discussed above, the thermodynamic exchange constants support a strong role for S in the mass transfer of Cu between haplogranite melt and aqueous vapor and brine.

The S-free data reported here agree well with the data presented in Candela and Holland (1984). Their study of Cu partitioning between silicate melt and aqueous supercritical fluid at 140 MPa, 750 °C and NNO yields a calculated $K_{Cu,Na_{140MPa}}^{v/m} = 24 \pm 18$ (1σ; $n = 9$). The two data sets are statistically indistinguishable at an alpha value of 0.01 (same variance and same mean). Thus, the exchange of Cu between melt and aqueous vapor does not change significantly over the temperature range 750–800 °C at 140 MPa. Williams et al. (1995) report values of $K_{Cu,Na}^{aqm/m}$, where aqm stands for aqueous mixture, at 100 MPa and 800 °C and 50 MPa and 850 °C based on experiments in a S-free melt–vapor–brine system. Note that the values of $K_{Cu,Na}^{aqm/m}$ are calculated by using Cu and Na concentrations in a quenched aqueous mixture of vapor and brine. They report values ($\pm 1\sigma$) $K_{Cu,Na}^{aqm/m} = 11 \pm 6$ and 215 ± 73, respectively. Williams et al. (1995) compare their data to Candela and Holland (1984) and note the strong increase in Cu–Na exchange at 100 MPa relative to the lower and higher pressures of 50 and 140 MPa. They evaluate hypotheses involving melt polymerization, aqueous phase density variation and chloride retention in the silicate melt and conclude that the maximum in $K_{Cu,Na}^{aqm/m}$ at 100 MPa results from a combination of decreasing water solubility with decreasing pressure coupled with either an increase in the chloride concentration of the melt or a decrease in the density of the vapor phase with decreasing pressure. Williams et al. (1995) note that many porphyry-Cu deposits formed at pressures on the order of 100 MPa and, thus, the maximum $K_{Cu,Na}^{aqm/m}$ value of 100 MPa agrees with field data.

In order to compare the new S-free data with the data and conclusions of Williams et al. (1995), we have calculated true $K_{Cu,Na_{100MPa}}^{v/m}$ by using their data set and inferring the Na concentration of vapor based on phase relations in the NaCl–H_2O system (Bodnar et al., 1985) at 100 and 50 MPa and 800 °C. We used a Na concentration of 6700 μg/g (assuming a molar ratio of Na:K:H of unity at 2.0 wt% NaCl eq.) in the vapor along with the melt concentrations of Na and Cu reported in Williams et al. (1995) to calculate a Cu concentration of the vapor. This yields a calculated value for $K_{Cu,Na_{100MPa}}^{v/m} = 18 \pm 2(1\sigma)$. This value is similar to the value determined herein of $K_{Cu,Na_{140MPa}}^{v/m} = 34 \pm 21(1\sigma)$ indicating that at between 50 and 100 MPa there is not a maximum in the value of $K_{Cu,Na}^{v/m}$ at 100 MPa. The same calculations were performed for the 100 MPa melt–brine data reported in Williams et al. (1995) by using again the reported concentrations of Na and Cu in the melt, a concentration of Na = 206,000 μg/g (assuming a molar ratio of Na:K:H of unity at 62 wt% NaCl eq.) in the brine based on Bodnar et al. (1985) and a concentration of Cu in the brine calculated by using the reported partition coefficient for Cu between melt and brine. These data yield a calculated $K_{Cu,Na_{100MPa}}^{b/m} = 71 \pm 8(1\sigma)$. This calculated exchange constant is more than twice as high as that reported herein ($K_{Cu,Na}^{b/m} = 33 \pm 22$; 1σ). Thus, the conclusion of Williams et al. (1995) that there is a maximum value of Cu–Na exchange at 100 MPa in the S-free brine–melt system is valid. We also performed the calculations for the 50 MPa data reported in Williams et al. (1995). The concentrations of Na and Cu in melt are from their study, the concentration of Cu in vapor was calculated from their reported vapor/brine partition coefficient (coupled with their reported brine/melt partition coefficient) and a Na concentration in vapor of 1363 μg/g (assuming Na:K:H of unity at 0.4 wt% NaCl eq.). These data yield a $K_{Cu,Na_{50MPa}}^{v/m} = 3.1 \pm 0.3(1\sigma)$. Following the same logic and by using a Na concentration in brine of 260,000 μg/g (77 wt% NaCl eq. assuming K:Na:H of unity), we calculate that $K_{Cu,Na_{50MPa}}^{b/m} = 3.4 \pm 0.3(1\sigma)$. These data demonstrate that a true maximum in $K_{Cu,Na}^{b/m}$ exists at 100 MPa and, thus, Cu partitioning from silicate melt to aqueous brine is strongest at this pressure.

We agree with Williams et al. (1995) that the relationship between $K_{Cu,Na}^{b/m}$ and pressure is not mere coincidence as the maximum in the exchange equilibria occurs at 100 MPa, corresponding the lithostatic depths at which

many porphyry-Cu ore deposits are known to form. However, the exchange of Cu and Na between S-free melt and vapor does not apparently exhibit a statistically relevant maximum across the pressure range 50 to 100 MPa. The results obtained here agree with the theoretical treatment of copper(I) chloride speciation and chalcopyrite solubility. Liu and McPhail (2005) used a revised HKF equation-of-state to demonstrate that temperature has a much stronger effect on chalcopyrite deposition than does pressure. Their results indicate that at a given temperature, decreasing pressure yields an increase of chalcopyrite solubility owing to the PT dependence of the log formation constant values for copper(I) chloride complexes. Thus, fluid cooling is the dominant cause of Cu-mineral precipitation in porphyry-type environments where fluid salinity is relatively constant. The S-bearing data presented here do not discount entirely the conclusions drawn from S-free data sets. However, data in the present study demonstrate that the presence of S increases the mass transfer of Cu from silicate melt to aqueous vapor at 140 MPa.

4.2. Geologic modeling

The presence of S is a salient feature of natural magmatic-hydrothermal systems and the data presented here demonstrate that S has a pronounced effect on the ability of volatile phases to scavenge Cu from silicate melt. As discussed by Williams-Jones and Heinrich (2005), the vast majority of published magmatic-hydrothermal ore deposit models invoke the presence of high-salinity, aqueous brine as the primary ore-metal transport agent. Henley and McNabb (1978) advocated a strong role for magmatic vapor to transport metals. However, their model was largely ignored owing to the knowledge, based on experimental data in S-free systems, that metal concentrations of aqueous magmatic-hydrothermal fluids increase linearly with the chloride concentration of the aqueous phase. The ability of magmatic vapor to transport significant quantities of metals, including Cu, has long been known from studies of geothermal systems and volcanic vapors. Our data confirm that aqueous brine can transport significant quantities of Cu and additionally the new data suggest the magmatic vapor may be as, if not more, efficient at scavenging Cu from silicate melt (cf. Candela and Piccoli, 1995; Williams-Jones and Heinrich, 2005). The ability of vapor to transport a greater absolute quantity of Cu owes to the high ratio of vapor to brine in most melt–vapor–brine systems (cf. Candela and Piccoli, 1995; Williams-Jones and Heinrich, 2005).

The geological significance of the data reported in this study can be evaluated with a mathematical model for the evolution of a volatile-saturated magmatic system. The mass transfer of Cu from a crystallizing melt to an exsolved volatile phase can be modeled using the equation:

$$E(\mathrm{Cu}) = \left[\frac{C^{\mathrm{l},0}_{\mathrm{H_2O}}}{C^{\mathrm{l,s}}_{\mathrm{H_2O}}}\right]^{\overline{D}_{\mathrm{Cu}}} \times \left[1 + \frac{\overline{D}_{\mathrm{Cu}}}{C^{\mathrm{l,s}}_{\mathrm{H_2O}} \times D^{\mathrm{aq/m}}_{\mathrm{Cu}}}\right]^{-1} \quad (15)$$

Table 9
Variables used in equations

Variable	Definition
m	Melt
v	Vapor
b	Brine
aq	Aqueous phase
f	Fugacity
$K^{a/b}_{i/j}$	The apparent exchange equilibrium constant for components i and j between phases a and b
C^{a}_{i}	The concentration of component i in phase a
E(Cu)	The efficiency with which Cu is scavenged from the melt by an exsolved volatile phase
$C^{\mathrm{l},0}_{\mathrm{H_2O}}$	The initial concentration of water in the silicate melt
$C^{\mathrm{l,s}}_{\mathrm{H_2O}}$	The concentration of water in the melt at water saturation
$\overline{D}_{\mathrm{Cu}}$	The bulk partition coefficient for Cu
$D^{\mathrm{aq/m}}_{\mathrm{Cu}}$	The Nernst-type partition coefficient for Cu between the aqueous fluid and the silicate melt

(Candela, 1986); variables are defined in Table 9. The calculation yields efficiencies between 0, no mass transfer of Cu to the volatile phase, and 1, complete mass transfer of Cu to the volatile phase. Efficiencies close to unity indicate the strong potential for Cu-porphyry formation, whereas efficiencies near zero suggest that conditions are not favorable for ore formation.

The master equation (Eq. (15)) was used to evaluate the effect of initial water concentration ($C^{\mathrm{l},0}_{\mathrm{H_2O}}/C^{\mathrm{l,s}}_{\mathrm{H_2O}}$) on the mass transfer of Cu. This constrains the total quantity of Cu scavenged by aqueous phases as a function of the crystallization time interval to reach water saturation. It allows us to evaluate the effect of pyrrhotite and magnetite crystallization by varying the value of $\overline{D}_{\mathrm{Cu}}$. Eq. (15) was designed for a constant $D^{\mathrm{aq/m}}_{\mathrm{Cu}}$ and fixed chlorine concentration. The calculations were done using a constant value of $D^{\mathrm{aq/m}}_{\mathrm{Cu}}$ and assuming the system is saturated with both vapor and brine; thus, fixing the chlorine concentration in each volatile phase. We performed the calculations by using pyrrhotite/melt partition coefficients at high ($\log f_{\mathrm{S_2}} = -1$; Jugo et al., 1999) and low ($\log f_{\mathrm{S_2}} = -3$; this study) sulfur fugacities. The vapor/melt and brine/melt partition data reported in the current study are used in all calculations. First, we discuss the model results calculated for low $f_{\mathrm{S_2}}$ conditions.

The following partition coefficient values were used in the calculations: $D^{\mathrm{b/m}}_{\mathrm{Cu}} = 443$, $D^{\mathrm{v/m}}_{\mathrm{Cu}} = 315$, $D^{\mathrm{po/m}}_{\mathrm{Cu}} = 174$, $D^{\mathrm{mt/m}}_{\mathrm{Cu}} = 2$. An initial concentration of 60 μg/g Cu (Gill, 1981) in melt was used in all calculations. The results are shown in Fig. 4 for the case of vapor. The first case includes mass fractions of pyrrhotite and magnetite of 0.025% and 1.7%, respectively, yields a $\overline{D}_{\mathrm{Cu}} = 0.0775$. The calculated E(Cu) ranges from 83% to 99%. The second case uses slightly higher mass fractions of pyrrhotite (0.1%) and magnetite (8.6%) yielding a calculated value of $\overline{D}_{\mathrm{Cu}} = 0.346$. The E(Cu) in vapor ranges from 44% to 98%. These results indicate that the Cu-scavenging potential of aqueous vapor is a strong function of the relative amounts of pyrrhotite and magnetite present in the

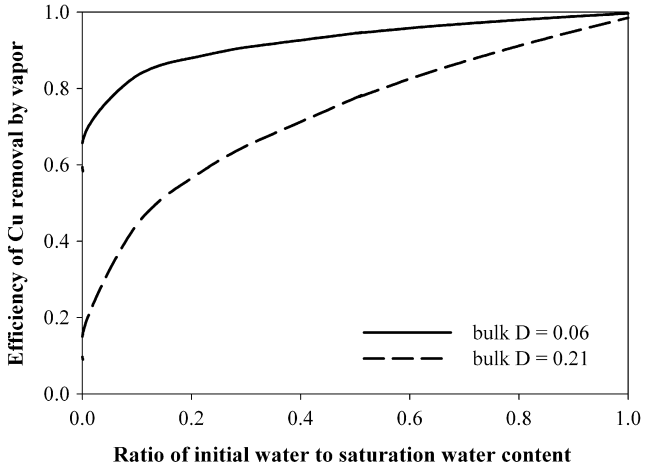

Fig. 4. The efficiency of Cu removal by aqueous vapor as a function of the $C^{l,0}_{H_2O}/C^{l,s}_{H_2O}$ in the silicate melt. The solid line represents the percent Cu (on a scale from 0 to 1) that aqueous vapor can scavenge from a degassing rhyolite melt if the bulk distribution coefficient ($\overline{D}$) for Cu in a melt-magnetite–pyrrhotite-vapor assemblage ($\overline{D}$) is 0.06. The dashed line is the calculated efficiency of Cu removal by the vapor for a $\overline{D}$ of 0.21. The figure indicates that increasing the modal abundance of magnetite and pyrrhotite, hence increasing $\overline{D}$, at a given $C^{l,0}_{H_2O}/C^{l,s}_{H_2O}$ ratio, decreases the total quantity of Cu which can be scavenged from the melt by the vapor phase. The model calculations for brine yield similar numbers and, thus, only the results for vapor are shown here.

fractionating assemblage and the initial $C^{l,0}_{H_2O}/C^{l,s}_{H_2O}$ ratio of the melt. A melt with an initial $C^{l,0}_{H_2O}/C^{l,s}_{H_2O}$ of 0.5 yields a vapor which can scavenge between 77% Cu (high modal abundance of pyrrhotite and magnetite) and 94% Cu (low modal abundance of pyrrhotite and magnetite) from the melt. Note that the calculation assumes a constant bulk partition coefficient. If the relative quantities of pyrrhotite and magnetite crystallizing from silicate melt decrease with time the efficiencies of removal will increase.

The model data at higher f_{S_2} reveal a different story. In the absence of vapor/melt and brine/melt partitioning data at the f_{S_2} reported in Jugo et al. (1999), we used the vapor/melt and brine/melt data reported here. These partition coefficients may change with increasing f_{S_2}, but the goal here is simply to illustrate the potential effect of the higher pyrrhotite/melt partition coefficient (i.e., $D^{po/m}_{Cu} = 2600$) reported by Jugo et al. (1999). The E(Cu) ranges from 20% to 95% for mass fractions of pyrrhotite and magnetite of 0.025% and 1.7%, respectively, yielding a $\overline{D}_{Cu} = 0.68$. The E(Cu) ranges from 0.1% to 85% for mass fractions of pyrrhotite and magnetite of 0.1% and 8.6%, respectively, yielding a $\overline{D}_{Cu} = 2.7$. Thus, at high f_{S_2} conditions the ability of magmatic vapor to scavenge Cu from the melt is maximized only for melts with high initial H_2O. For example, a melt intruding with a $C^{l,0}_{H_2O}/C^{l,s}_{H_2O} = 0.5$ (i.e., initially contains 2.5 wt% H_2O and water solubility is 5 wt% H_2O) the vapor can scavenge only 12 mass% Cu from the melt. A melt with an initial $C^{l,0}_{H_2O}/C^{l,s}_{H_2O} = 0.8$ exsolves a vapor which can scavenge 46% Cu, by mass, from the melt.

To illustrate the effect of these E(Cu) data for the vapor phase, we can evaluate how much Cu may be scavenged by aqueous vapor from a hypothetical 1 km^3 silicate melt with a density of 2700 kg/m^3. Such a melt contains a total of 1.62×10^8 kg Cu at 60 μg/g Cu. Even at the highest reasonable mass fractions of pyrrhotite and magnetite (i.e., highest $\overline{D}_{Cu}$), aqueous vapor exsolved from a low f_{S_2} melt with a low initial water concentration ($C^{l,0}_{H_2O}/C^{l,s}_{H_2O} = 0.2$) can scavenge 7.1×10^4 metric tons of Cu from a 1 km^3 volume of silicate melt. Note that this is a minimum estimate. If the melt is initially wetter and/or less pyrrhotite and magnetite are present, the vapor can scavenge greater quantities of Cu. A 10 km^3 silicate melt has the potential to supply 8.1×10^5 metric tons of Cu to an aqueous vapor. The calculations at higher f_{S_2} conditions demonstrate that vapor scavenges significantly less Cu from silicate melt. Vapor exsolved from a 10 km^3 melt with a $C^{l,0}_{H_2O}/C^{l,s}_{H_2O} = 0.2$ can scavenge 5.2×10^5 tons Cu from the melt. The initial $C^{l,0}_{H_2O}/C^{l,s}_{H_2O}$ must be on the order of 0.4 for the high f_{S_2} vapor to scavenge 8.2×10^5 tons of Cu, a value achieved by the low f_{S_2} vapor exsolved from melt with an initial $C^{l,0}_{H_2O}/C^{l,s}_{H_2O} = 0.2$. Note that the aqueous vapor used in these calculations contains on the order of 9 wt% NaCl eq. This vapor salinity agrees well with the salinity of aqueous vapor fluid inclusions intimately associated with mineralization at the world-class Cu-, Au-porphyry deposit at Grasberg, Irian Jaya, Indonesia, which contain, on average, 7.4 ± 3 wt% NaCl eq. A magmatic vapor with a lower salinity will scavenge less Cu and, thus, the calculated Cu tonnages will decrease.

Silicate melts may exsolve brine prior to vapor, as documented by Cline and Bodnar (1994) and Cline and Vanko (1995) at the Questa porphyry-molybdenum mine in New Mexico, U.S.A. In the case of a low-f_{S_2} silicate melt with mass fractions of pyrrhotite and magnetite of 0.025% and 1.7%, respectively, and an initial $C^{l,0}_{H_2O}/C^{l,s}_{H_2O} = 0.2$, the brine can scavenge between 84% and 99% Cu as the $C^{l,0}_{H_2O}/C^{l,s}_{H_2O}$ ratio increases from 0.2 to 1. If pyrrhotite and magnetite constitute 0.1% and 8.6% of the fractionating assemblage, respectively, the brine can scavenge 44% to 98% Cu from silicate melt. The efficiencies of removal for vapor and brine overlap and, thus, by using the same hypothetical 1 km^3 melt as above, the model results suggest that brine has the potential to scavenge a minimum of 9.8×10^4 metric tons of Cu. The calculated efficiencies for vapor and brine overlap owing to the statistically similar vapor/melt and brine/melt partition coefficients. Model calculations assuming a high f_{S_2} system indicate that brine can scavenge between 20% and 97% Cu from a melt with magnetite and pyrrhotite constituting 0.025 and 1.7 modal%, respectively. For higher modal abundances of 0.1% and 8.6%, the brine can scavenge between 0.1% and 89% Cu from the fractionating silicate melt. Again, these efficiencies are dramatically lowered because of the higher $\overline{D}_{Cu}$ in the high f_{S_2} system.

One should not interpret the calculations here as demonstrating that pyrrhotite destroys the ore-forming potential an evolving magmatic system at high f_{S_2}. As discussed in Boudreau and Meurer (1999), sulfide crystals and/or immiscible sulfide melt formed prior to volatile saturation

can act as efficient pre-concentrating agents which may promote the mineralization process. Their chromatographic model calls upon infiltration and reaction of the ascending volatile phase with stratigraphically higher, volatile-undersaturated melt ± crystals. Pyrrhotite and magnetite crystals will gravitationally settle through the melt column only in the first 25% crystallization (Marsh, 1981). In the case of a melt undergoing crystallization induced water saturation, volatile exsolution will occur first in the magma volumes with the highest crystal density and once formed, the volatile phase will react with both the local melt and pyrrhotite, and other crystals. Volatile exsolution will also promote sulfide resorption. Boudreau and McCallum (1992) suggest that sulfide resorption from the early cumulus assemblage of magma bodies may increase significantly the ore-forming potential of a given magmatic system. Resorption of the sulfides is driven by the exsolution of a volatile phase which causes auto-oxidation of the magma and sulfur as H_2S and SO_2. The ascending aqueous fluid may also be resorbed into hotter, volatile-undersaturated melt. This process will amplify the local H_2O, Cl, S and Cu concentrations in the melt. This process probably occurs repeatedly as the volatile front sweeps continually upward through the magma. Once the local melt volume reaches volatile saturation, Cl, S and Cu contained in the melt and/or previously precipitated sulfides can be scavenged by the volatile phase. The study by Halter et al. (2005) demonstrate that this process may occur in natural magmas by noting the change in Cu concentrations of silicate and sulfide melt inclusions trapped before and after the melt reached volatile saturation. Their data demonstrate a strong depletion of Cu in silicate melts closely associated with sulfide melts, the latter being strongly enriched with up to 9 wt% Cu. The sulfides formed after volatile exsolution have notably lower Cu concentrations.

Keith et al. (1997) and Larocque et al. (2000) propose that volatile saturation and concomitant sulfide destabilization were responsible for ore mineralization in the Bingham porphyry-Cu, -Mo deposit, Utah. Their studies document the strong enrichment of Cu (and Ag) in magmatic sulfides present in lattices which are genetically linked (i.e., comagmatic) to the ore-related intrusions. Early sulfides in the ore-related magma would also be expected to contain high concentrations of Cu. The exsolution of a volatile phase may have caused large-scale resorption or dissolution of magmatic sulfides which would supply significant quantities of Cu to the evolving magmatic volatile phase(s) (Keith et al., 1997). Hattori (1993) has also discussed the resorption of sulfides owing to influx of SO_2-rich fluids which oxidize the sulfides during magma recharge. Thus, the presence of pyrrhotite, and or other sulfide phases, in the early cumulus assemblage of a high f_{S_2} magma does not, in and of itself, thwart the ore-forming potential of that system.

The efficiencies of removal were also calculated for the S-free assemblage to elucidate the effect of S on the mass transfer of Cu from melt into exsolved volatile phases. The calculations were performed at identical conditions as above except that partitioning data from the S-free experiments were used. Values for $D_{Cu}^{b/m}$ and $D_{Cu}^{v/m}$ of 200 and 63 were used in the calculations. The value of $\overline{D}_{Cu}$ was modified to reflect only magnetite as part of the crystallizing assemblage. The E(Cu) for vapor ranges from 72% to 95% and for brine from 74% to 98% with a mass fraction of magnetite ranging of 1.8%. The E(Cu) for vapor ranges from 64% to 93% and for brine from 67% to 98% with a mass fraction of magnetite ranging of 8.6%. These data demonstrate that S-free vapor and brine may scavenge significant quantities of Cu from a fractionating melt. However, the presence of S in natural magmatic systems makes the results of the S-bearing calculations more realistic.

5. Implications

The new results have important implications for the development of Cu-porphyry systems. The calculated efficiencies demonstrate that both vapor and brine can scavenge significant quantities of Cu from melt even if reasonable mass fractions of magnetite and pyrrhotite are part of the early fractionating assemblage. While the efficiencies were calculated using data generated from experiments at a single P and T, the results are applicable generally to other magmatic conditions. If the solid phases are completely removed from the magma greater than 50% of the Cu in the melt is available to be scavenged by a volatile phase(s). Melts with a higher initial water concentration favor the development of larger Cu-porphyry systems. If a melt saturates with vapor and/or brine early, the total quantity of Cu scavenged from the melt can easily supply enough Cu to form a world-class Cu-porphyry deposit.

The intimate association of co-existing vapor and brine fluid inclusions with Cu mineralization in many porphyry-Cu ore deposits suggests that both volatile phases may be important in advecting Cu to the deposits, as suggested by overlapping metal ratios in both vapor and brine inclusions with bulk ore at Grasberg (Ulrich et al., 1999). Considering that the mass fraction of vapor typically exceeds significantly that of brine in degassing magmatic systems (Candela and Piccoli, 1995; Williams-Jones and Heinrich, 2005), the new data reported here for Cu between vapor and melt suggest that the vapor phase may be the dominant agent of Cu mass transfer to porphyry-Cu deposits. Heinrich et al. (1992) report that vapor fluid inclusions associated with mineralization in the Mole Granite, Australia, contain higher concentrations of Cu than do co-existing aqueous brine fluid inclusions. Ulrich et al. (1999) report higher Cu concentrations in vapor relative to coexisting brine in boiling assemblages associated with Cu and Au mineralization at both the Bajo de la Alumbrera, Argentina and Grasberg, Irian Jaya, Indonesia porphyry deposits. The data in this study suggest that S enhances the mass transfer of Cu into vapor, albeit the vapor/brine partition coefficient remains less than one. Additional experiments at higher f_{S_2} are in progress to determine if increasing this

variable may further enhance the mass transfer of Cu from melt into vapor.

In addition to these natural examples of vapor and brine partitioning, one must remember that the vapor phase in most vapor- + brine-saturated magmatic systems constitutes the higher total mass of the two-phase aqueous fluid system. Additionally, at pressures <100 MPa, the exsolution of a single, low-salinity vapor is expected for high mass ratios of H_2O/Cl (Candela and Piccoli, 1995). As volatile exsolution continues, the chloride concentration of the melt increases and eventually the melt exsolves a brine which equilibrates with melt and vapor (Burnham, 1979; Bodnar et al., 1985; Cline and Bodnar, 1991; Candela and Piccoli, 1995; Cline, 1995; Webster et al., 1999; Ulrich et al., 2001; Audétat and Pettke, 2003). In our experiments the vapor to brine mass ratio is on the order of 95 to 1. Thus, the partition coefficients reported in this study for a S-bearing melt–vapor–brine–pyrrhotite–magnetite system and the mass ratio of vapor to brine suggest that the vapor phase may be significantly more important in advecting Cu from a fractionating silicate melt into the overlying porphyry environment. A detailed review of the importance of the vapor phase in advecting metals is discussed at length in Williams-Jones and Heinrich (2005).

6. Conclusions

Data in this study constrain the partitioning of Cu in a melt–vapor–brine–pyrrhotite–magnetite assemblage at 800 °C, 140 MPa, f_{O_2} = NNO, $\log f_{S_2} = -3.0$, $\log f_{H_2S} = -1.3$ and $\log f_{SO_2} = -1$. Calculated partition coefficients for Cu between S-free melt and vapor, S-free melt and brine and S-free vapor and brine agree broadly with previous studies in haplogranite-NaCl–KCl–HCl–H_2O aqueous volatile phase systems. The partition coefficients for Cu between Cl- and S-bearing melt and vapor, melt and brine and vapor and brine are notably elevated relative to those in the S-free system. The systematic increase in these partition coefficients in the presence of S suggests that a Cu-complexing sulfur ligand is responsible for the enhanced partitioning of Cu into the vapor. However, data here do not elucidate the speciation of Cu in S-bearing aqueous fluids. The reported Cu concentrations in magnetite and pyrrhotite suggest that the Cu-ore potential of a silicate melt is enhanced if volatile saturation occurs early in the case of crystallization-induced water saturation. The similar partition coefficients for Cu between vapor and melt and brine and melt in the S-bearing assemblage suggest that vapor may be much more important than previously thought in scavenging Cu from a fractionating magma and advecting the Cu to the superjacent magmatic environment where ore deposition occurs.

Acknowledgments

This work was partially supported by National Science Foundation grants: EAR 0309967 (P.A.C. and P.M.P.), EAR 9909576 (P.A.C. and P.M.P.) and EAR 0125805 (P.A.C. and P.M.P.); EAR 9810244 (P.M.P. and others). We thank Mark Frank and Andy Campbell and Associate Editor Ed Ripley for their thorough and constructive reviews which strengthened significantly the substance of the manuscript. The Isotope Geochemistry and Mineral Resources group at ETH acknowledges continued support from the Swiss National Science Foundation. A.C.S. thanks the Department of Geoscience and College of Sciences at UNLV for a first-year reduced teaching load which allowed him to write this manuscript. A.C.S. thanks Alicia, Abigail, James, Laura and Ethan for their support.

Associate editor: Edward M. Ripley

References

Acosta-Vigil, A., London, D., Morgan, G.B., Dewers VI, T.A., 2003. Solubility of excess alumina in hydrous granitic melts in equilibrium with peraluminous minerals at 700–800 °C and 200 MPa, and applications of the aluminum saturation index. *Contrib. Mineral. Petrol.* **146**, 100–119.

Anderko, A., Pitzer, K.S., 1993. Equation-of-state representation of phase equilibria and volumetric properties of the system NaCl–H_2O above 573 K. *Geochim. Cosmochim. Acta* **57**, 1657–1680.

Audétat, A., Pettke, T., 2003. The magmatic-hydrothermal evolution of two barren granites: a melt and fluid inclusion study of the Rito del Medio and Cañada Pinabete plutons in northern New Mexico (USA). *Geochim. Cosmochim. Acta* **67**, 97–121.

Audetat, A., Günther, D., Heinrich, C.A., 1998. Formation of a magmatic hydrothermal ore deposit; insights in with LA-ICP-MS analysis of fluid inclusions. *Science* **279**, 2091–2094.

Baker, T., Achterberg, E.V., Ryan, C.G., Lang, J.R., 2004. Composition and evolution of ore fluids in a magmatic-hydrothermal skarn deposit. *Geology* **32**, 117–120.

Belonoshko, A.B., Shi, P.F., Saxena, S.K., 1992. A FORTRAN-77 program for calculation of Gibbs free energy and volume of C–H–O–S–N–Ar mixtures. *Comput. Geosci.* **18**, 1267–1269.

Bodnar, R.J., Vityk, M.O., 1994. Interpretation of microthermometric data for H_2O NaCl fluid inclusions. In: De Vivo, B., Frezzotti, M.L. (Eds.), *Fluid Inclusions in Minerals, Methods and Applications*. Virginia Polytechnic Institute, VA, pp. 117–130.

Bodnar, R.J., Burnham, C.W., Sterner, S.M., 1985. Synthetic fluid inclusions in natural quartz. III. Determination of phase equilibrium properties in the system H_2O–NaCl to 1000 °C and 1500 bars. *Geochim. Cosmochim. Acta* **49**, 1861–1873.

Boudreau, A.E., McCallum, I.S., 1992. Concentration of platinum-group elements by magmatic fluids in layered intrusions. *Econ. Geol.* **87**, 1830–1848.

Boudreau, A.E., Meurer, W.P., 1999. Chromatographic separation of the platinum-group elements, gold, base metals and sulfur during degassing of a compacting and solidifying crystal pile. *Contrib. Min. Petrol.* **134**, 174–185.

Burnham, C.W., 1979. Magmas and hydrothermal fluids. In: Barnes, H.L. (Ed.), *Geochemistry of Hydrothermal Ore Deposits*. Wiley, New York, pp. 71–136.

Candela, P.A., 1986. Generalized mathematical models for the fractional evolution of vapor from magmas in terrestrial planetary crusts. In: Saxena, S.K. (Ed.), *Advances in Physical Geochemistry*, 6. Springer-Verlag, New York, pp. 362–396.

Candela, P.A., Holland, H.D., 1984. The partitioning of copper and molybdenum between melts and aqueous fluids. *Geochim. Cosmochim. Acta* **48**, 373–380.

Candela, P.A., Piccoli, P.M., 1995. Model ore-metal partitioning from melts into vapor and vapor/brine mixtures. In: Thompson, J.F.H.

(Ed.), *Magmas, Fluids, and Ore Deposits*, 23. Mineralogical Association of Canada Short Course, pp. 101–128.

Candela, P.A., Piccoli, P.M., 2005. In: Hedenquist, J.W., Thompson, J.F.H., Goldfarb, R.J., Richards, J.P. (Eds.), Magmatic Processes in the Development of Porphyry-type Ore Systems. Econ. Geol. vol. 100th Anniv., pp. 25–38.

Chou, I.C., 1987a. Oxygen buffer hydrogen sensor techniques at elevated pressures and temperatures. In: Ulmer, G.C., Barnes, H.L. (Eds.), Hydrothermal Experimental Techniques, pp. 61–99.

Chou, I.C., 1987b. Phase relations in the system NaCl–KCl–H_2O: III, solubilities of halite in vapor-saturated liquids above 445 °C and redetermination of phase equilibrium properties in the system NaCl–H_2O to 1000 °C and 1500 bars. *Geochim. Cosmochim. Acta* **51**, 1965–1975.

Clemente, B., Scaillet, B., Pichavant, M., 2004. The solubility of sulphur in hydrous rhyolitic melts. *J. Petrol.* **45** (11), 2171–2196.

Cline, J.S., 1995. Genesis of porphyry copper deposits: the behaviour of water, chloride and copper in crystallizing melts. *Arizona Geol. Soc. Dig.* **20**, 69–82.

Cline, J.S., Bodnar, R.J., 1991. Can economic porphyry copper mineralization be generated by a typical calc-alkaline melt? *J. Geophys. Res.* **96**, 8113–8116.

Cline, J., Bodnar, R., 1994. Direct evolution of a brine from a crystallizing silicic melt at the Questa, New Mexico, Molybdenum Deposit. *Economic Geology* **89**, 1780–1802.

Cline, J.S., Vanko, D.A., 1995. Magmatically generated saline brines related to molybdenum at Questa, New Mexico, USA. In: Thompson, J.F.H. (Ed.), *Magmas, Fluids, and Ore Deposits: Mineralogical*, vol. 23. Association of Canada Short Course Series, Victoria, BC, Canada, pp. 153–174.

Dilles, J.H., 1987. Petrology of the Yerington Batholith, Nevada; evidence for evolution of porphyry copper ore fluids. *Economic Geology* **82**, 1750–1789.

Drummond, S.E., Ohmoto, H., 1985. Chemical evolution and mineral deposition in boiling hydrothermal systems. *Econ. Geol.* **80**, 126–147.

Eastoe, C.J., 1982. Physics and chemistry of the hydrothermal system at the Panguna porphyry copper deposit, Bougainville, Papua New Guinea. *Econ. Geol.* **77**, 127–153.

Ewart, A., Griffin, W.L., 1994. Application of proton-microprobe data to trace-element partitioning in volcanic rocks. *Chem. Geol.* **117** (1-4), 251–284.

Frank, M.R., 2001. An experimental investigation of ore metals in silicate melt-volatile phase systems. Ph.D. dissertation, University of Maryland.

Gill, J., 1981. *Orogenic Andesites and Plate Tectonics*. Springer-Verlag, New York, 390 pp.

Günther, D., Frischknecht, R., Heinrich, C.A., Kahlert, H.J., 1997. Capabilities of an Argon fluoride 193 nm Excimer laser ablation inductively coupled plasma mass spectrometry microanalysis of geological materials. *J. Anal. Atom. Spec.* **12**, 939–944.

Günther, D., Audétat, A., Frischknecht, A., Heinrich, C.A., 1998. Quantitative analysis of major, minor, and trace elements in fluid inclusions using laser ablation-inductively coupled plasma mass spectrometry. *J. Anal. Atom. Spec.* **13**, 263–270.

Halter, W.E., Pettke, T., Heinrich, C.A., Rothen-Rutishauser, B., 2002. Major to trace element analysis of melt inclusions by laser-ablation ICP-MS: methods of quantification. *Chem. Geol.* **183**, 63–86.

Halter, W.E., Heinrich, C.A., Pettke, T., 2005. Magma evolution and the formation of porphyry Cu–Au ore fluids: evidence from silicate and sulfide melt inclusions. *Miner. Depos.* **39**, 845–863.

Hanley, J.J., Pettke, T., Mungall, J.E., Spooner, T.C., 2005. The solubility of platinum and gold in NaCl brines at 1.5 kbar, 600 to 800 °C: a laser ablation ICP-MS pilot study of synthetic fluid inclusions. *Geochim. Cosmochim. Acta* **69** (10), 2593–2611.

Harris, A.C., Kamenetsky, V.S., White, N.C., van Achterberg, E., Ryan, C.B., 2003. Melt inclusions in veins: linking magmas and porphyry Cu deposits. Science, 302, 21909-2111. Between magmatic brine and vapor: a fluid inclusion study using PIXE microanalysis. *Econ. Geol.* **87**, 1566–1583.

Hattori, K., 1993. High-sulfur magma, a product of fluid discharge from underlying mafic magme: evidence from Mount Pinatubo, Philippines. *Geology* **21**, 1083–1086.

Hedenquist, J.W., Lowenstern, J.B., 1994. The role of magmas in the formation of hydrothermal ore deposits. *Nature* **370**, 519–527.

Heinrich, C.A., Ryan, C.G., Mernagh, T.P., Eadington, P.J., 1992. Segregation of ore metals between magmatic brine and vapor. *Econ. Geol.* **87**, 1566–1583.

Heinrich, C.A., Günther, D., Audétat, A., Ulrich, T., Frischknecht, R., 1999. Metal fractionation between magmatic brine and vapor, determined by microanalysis of fluid inclusions. *Geology* **27**, 755–758.

Heinrich, C.A., Pettke, T., Halter, W.E., Aigner-Torres, M., Audétat, A., Günther, D., Hattendorf, D., Bleiner, D., Guillong, M., Horn, I., 2003. Quantitative multi-element analysis of minerals, fluid and melt inclusions by Laser-Ablation Inductively-Coupled-Plasma Mass Spectrometry. *Geochim. Cosmochim. Acta* **67**, 3473–3497.

Henley, R.W., McNabb, A., 1978. Magmatic vapor plumes and groundwater interaction in porphyry copper emplacement. *Econ. Geol.* **73**, 1–20.

Hewitt, W.P., 1968. Geology and mineralization of the main mineral zone of the Santa Eulalia district, Chihuahua, Mexico. *Soc. Mining Eng. AIME Trans.* **241**, 228–260.

Holland, H.D., 1972. Granites, solutions, and base metal deposits. *Econ. Geol.* **67**, 281–301.

Huebner, J.S., Sato, M.S., 1970. The oxygen fugacity-temperature relationships of manganese oxide and nickel oxide buffers. *Am. Mineral.* **55**, 934–938.

Jugo, P.J., Candela, P.A., Piccoli, P.M., 1999. Linearly independent conditions of chemical equilibrium for the partitioning of ore metals in melt-crystal-volatile phase systems: applications to mineral exploration. Second International Symposium on Granites and Associated Mineralizations; Salvador, Brazil. *Lithos* 46, 573–589.

Jugo, P.J., Candela, P.A., Piccoli, P.M., 1999. Magmatic sulfides and Au:Cu ratios in porphyry deposits: an experimental study of copper and gold partitioning at 850 °C, 100 MPa in a haplogranitic melt–pyrrhotite–intermediate solid solution – gold metal assemblage, at gas saturation. *Lithos* **46**, 573–589.

Keith, J.D., Whitney, J.D., Hattori, K., Ballantyne, G.H., Christiansen, E.H., Barr, D.L., Cannan, T.M., Hook, C.J., 1997. The role of magmatic sulfides and mafic alkaline magmas in the Bingham and Tintic mining districts, Utah. *J. Petrol.* **38**, 1679–1690.

Larocque, A.C.L., Stimac, J.A., Keith, J.D., Huminicki, M.A.E., 2000. Destabilization of immiscible sulfides in silicate melts: implications for the contribution of metals and sulfur to magmatic ore-forming fluids. IAVCEI General Assembly, 18–22 July, Bali, p. 120 (abstract).

Liu, W., McPhail, D.C., 2005. Thermodynamic properties of copper chloride complexes and copper transport in magmatic-hydrothermal solutions. *Chem. Geol.* **221**, 21–39.

Longerich, H.P., Günther, D., Jackson, S.E., 1996. Laser ablation inductively coupled plasma mass spectrometric transient signal data acquisition and analyte concentration calculation. *J. Anal. Atom. Spectr.* **9**, 899–904.

Lowenstern, J.B., 1993. Evidence for a copper-bearing fluid in magma erupted at the Valley of Ten Thousand Smokes, Alaska. *Contrib. Mineral. Petrol.* **114**, 409–421.

Lynton, S.J., Candela, P.A., Piccoli, P.M., 1993. An experimental study of the partitioning of copper between pyrrhotite and a high silica rhyolitic melt. *Econ. Geol.* **88**, 901–915.

Marsh, B.D., 1981. On the crystallinity, probability of occurrence, and rheology of lava and magma. *Contrib. Min. Petrol.* **78**, 85–98.

Morgan VI, G.B., London, D., 1996. Optimizing the electron microprobe analysis of hydrous alkali aluminosilicate glasses. *Am. Mineral.* **81**, 1176–1185.

Mountain, B.W., Seward, T.M., 1999. The hydrosulphide/sulphide complexes of copper(I): experimental determination of stoichiometry

and stability at 25 °C and reassessment of high temperature data. *Geochim. Cosmochim. Acta* **63**, 11–29.

Pettke, T., Halter, W.E., Webster, J.D., Aigner-Torres, M., Heinrich, C.A., 2004. Accurate quantification of melt inclusion chemistry by LA-ICPMS: a comparison with EMP and SIMS and advantages and possible limitations of these methods. *Lithos* **78**, 333–361.

Pokrovski, G.S., Roux, J., Harrichoury, J.-Cl., 2005. Fluid density control on vapor–liquid partitioning of metals in hydrothermal systems. *Geology* **33**, 657–660.

Roedder, E., 1972. Compositions of fluid inclusions. U.S. Geological Survey Professional Paper 440, 164 p.

Roedder, E., 1984. Fluid Inclusions. *Rev. Mineral.* **12**, 644 pp.

Ryan, C.G., McInnes, B.M., Williams, P.J., Dong, G., Win, T.T., Yeats, C.J., 2001. Imaging fluid inclusion content using the new CSIRO-GEMOC nuclear microprobe. *Nucl. Intr. Meth.* **B181**, 570–577.

Simon, A.C., Pettke, T., Candela, P.A., Piccoli, P.M., Heinrich, C.A., 2003. Experimental determination of Au solubility in rhyolite melt and magnetite: constraints on magmatic Au budgets. *Am. Mineral.* **88**, 1644–1651.

Simon, A.C., Pettke, T., Candela, P.A., Piccoli, P.M., Heinrich, C.A., 2004. Magnetite solubility and iron transport in magmatic-hydrothermal environments. *Geochim. Cosmochim. Acta* **68**, 4905–4914.

Simon, A.C., Pettke, T., Candela, P.A., Piccoli, P.M., Heinrich, C.A., 2005. Gold partitioning in melt–vapor–brine systems. *Geochim. Cosmochim. Acta* **69**, 3321–3335.

Simon, A.C., Frank, M., Pettke, T., Candela, P.A., Piccoli, P.M., Heinrich, C., Glascock, M., 2006. An evaluation of synthetic fluid inclusions for the purpose of trapping equilibrated coexisting immiscible fluids at experimental PVTX conditions. *Am. Mineral.*, in press.

Stimac, J., Hickmott, D.D., 1994. Trace-element partition coefficients for ilmenite, orthopyroxene, and pyrrhotite in rhyolite determined by micro-PIXE analysis. *Chem. Geol.* **117**, 313–330.

Stuller, B., 2001. The partitioning behavior of manganese, cobalt, nickel, zinc, molybdenum, tungsten and gold between pyrrhotite and a rhyolitic melt. Unpublished M.S. Thesis, University of Maryland.

Toulmin, P., Barton, P.B., 1964. A thermodynamic study of pyrite and pyrrhotite. *Geochim. Cosmochim. Acta* **28**, 641–671.

Ulrich, T., Günther, D., Heinrich, C.A., 1999. Gold concentrations of magmatic brines and the metal budget of porphyry copper deposits. *Nature* **399**, 676–679.

Ulrich, T., Günther, D., Heinrich, C.A., 2001. Evolution of a porphyry Cu–Au deposit, based on LA-ICP-MS analysis of fluid inclusions, Bajo de la Alumbrera, Argentina. *Econ. Geol.* **97**, 1888–1920.

Webster, J.D., Kinzler, R.J., Mathez, E.A., 1999. Chloride and water solubility in basalt and andesite melts and implications for magmatic degassing. *Geochim. Cosmochim. Acta* **63**, 729–738.

Westrich, H.R., Eichelberger, J.C., Hervig, R.I., 1991. Degassing of the 1912 Katmai magmas. *Geophys. Res. Lett.* **18**, 1561–1564.

Whitney, J.W., 1975. Vapor generation in a quartz monzonite magma: a synthetic model with application to porphyry copper deposits. *Econ. Geol.* **70**, 346–358.

Whitney, J.A., 1984. Fugacities of sulfurous gases in pyrrhotite-bearing magmas. *Am. Mineral.* **69**, 69–78.

Williams, T.J., Candela, P.A., Piccoli, P.M., 1995. The partitioning of copper between silicate melts and two-phase aqueous fluids: an experimental investigation at kbar, 800 °C and 0.5 kbar, 850 °C. *Contrib. Miner. Petrol.* **121**, 388–399.

Williams, T.J., Candela, P.A., Piccoli, P.M., 1997. Hydrogen-alkali exchange between silicate melts and two-phase aqueous mixtures; an experimental investigation. *Contrib. Min. Petrol.* **128**, 114–126.

Williams-Jones, A.E., Heinrich, C.A., 2005. In: Hedenquist, J.W., Thompson, J.F.H., Goldfarb, R.J., Richards, J.P. (Eds.), Vapor Transport of Metals and the Formation of Magmatic-hydrothermal Ore Deposits. Econ. Geol. vol. 100th Anniv., pp. 1287–1312.